Nonlinear Static and Dynamic Analysis of Marine Pipelines During Laying

G.F. Clauss, H. Weede and A. Saroukh
Institut für Schiffs-und Meerestechnik, Technische Universität Berlin

1. Introduction

The technique of offshore pipelaying is shown in Fig.1. Segments of steel pipe, weighted and protected by a concrete coating, are connected on board. A tensioner retains the pipeline on the moored vessel and supplies the required tension to the unsupported span. As the tensioner grips the pipe with a pair of caterpillar tracks, it can provide an axial pipe motion relative to the vessel to pay out pipe and to keep tension force oscillations within a permissible range. *(Langner and Ayers 1985)*. For limiting the pipe stress at the upper end of the span, the pipe is guided over a circular stinger equipped with rollers. Its radius corresponds at least to the maximum tolerable bending stress, and its length must ensure that the pipe lifts off smoothly well ahead of the lower end of the stinger to avoid an excessive bending moment peak at the last roller. In extremly deep water the pipe axis becomes so steep that the required stinger length may not be feasible for the S-method. In this case, the J-method is recommended: All welding equipment and the tensioner can be variably inclined to minimize the bending moment at the clamped end.

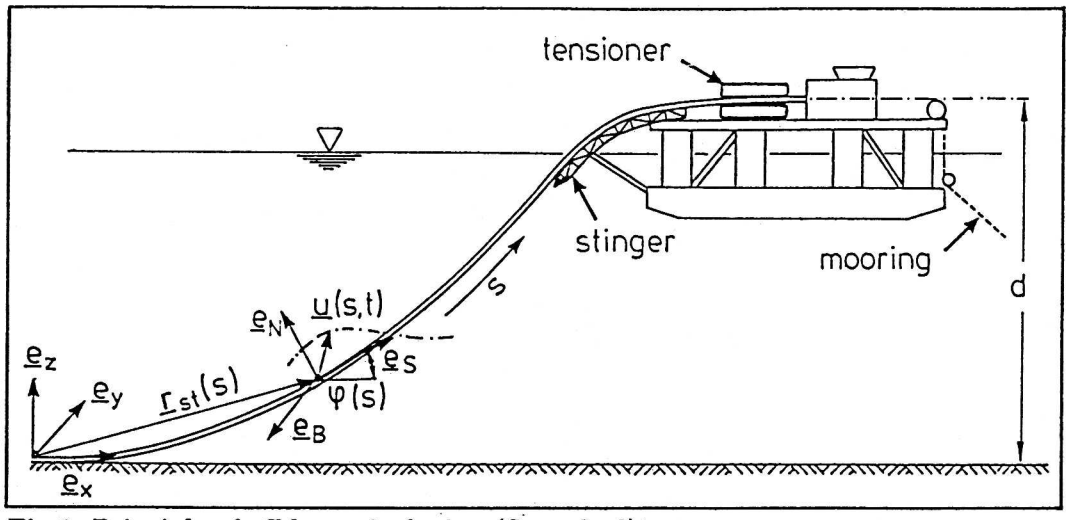

Fig.1: Principle of offshore pipelaying (S-method)

Only a few papers on the dynamics of pipelaying have been published up to now.

Kirk and Etok (1979) studied random-wave-induced motions of pipelines in the J-configuration. Their analysis is based on Morison's equation and spectral analysis of linearized responses in the first five modes of oscillation. Vessel motions and variations of axial tension are not considered. The pipe ends are assumed clamped or hinged.

Malahy (1986) developed a general purpose dynamic beam analysis method which is also valid for pipelaying. It is based on Hamilton's principle applied to a finite element model with oscillating local coordinate systems. Acceleration and velocity discretization for a time domain simulation is based on the trapezoidal integration rule. An inner loop solves the equation system at each timestep, and an outer loop improves the solution using Newton's method.

Clauss and Weede (1990) published a simplified version of the present method. Nonlinearities were simulated by offset effects in the frequency domain approach. This 'semi-nonlinear' method may still be interesting as a more simple alternative. It is based on large deflection circular beam theory *(Weede 1990)* which yields a differential equation for the radius vector of the oscillating pipe's axis (Table 1).

Vlahopoulos and Bernitsas (1990) expanded the same vector equation by adding some terms, e.g. for bending rotatory inertia and structural damping. A vector version of Galerkin's method is introduced together with a finite element discretization; thus, a coupled equation system with time dependent matrices is obtained. It is solved by means of Newmark's method. Special effort is devoted to accurately simulate the monolateral support of the pipe by both stinger and seabed, including soil friction. Their rigid soil model, however, neglects soil damping.

Weede (1990) published a large deflection dynamic analysis method for submerged slender beams excited by arbitrary line loads and boundary motions.

Two other publications on pipelaying analysis are only considering the static case, but with some interesting special effects. *Pedersen and Yan (1986)* include non-circular configurations, e.g. bundles of several pipes. *Oliver and Oñate (1985)* include sheer and nonlinear elasticity, e.g. plastic pipes. Both publications describe quite sophisticated three-dimensional numerical methods.

As a related topic, riser analysis should also be considered.

Gardner and Kotch (1976) presented the type of dynamic bending equation later used by *Hapel and Köhl (1980)* and also in the present paper. They introduced the assumption that the dynamic tension force depends on time only, but not on the curve length. The present paper applies this assumption to pipelaying. For details see *Weede (1990)* and *Kauderer (1958)*. Gardner and Kotch discuss the case that the dynamic tension force is known. In the present paper it is deduced from the vessel's motions together with the bending oscillations. Their method of solving the nonlinear problem is to gather all nonlinearities as an initially unknown load and to improve the solution iteratively.

Hapel and Köhl (1980) took advantage of the fact that the static tension force in a marine riser increases linearly from bottom to top. Dynamic tension and flexural rigidity are neglected. After linearizing the hydrodynamic drag, the dynamic bending equation is solved analytically using modified Bessel functions.

Frequency domain analysis performs quite poorly if one evaluates the linearized hydrodynamic damping parameter in time domain. The corresponding Eq. (19) in this paper is speeded up in practice with an approach presented by *Krolikowski and Gay (1980)* for irregular seaway as a Gaussian process *(Borgman 1969)*.

Cable dynamics differ from pipelaying due to both large axial strain and the absence of flexural rigidity. For the planar case, *Bliek and Triantafillou (1985)* present a linear and a nonlinear solution based on equilibrium methods. The nonlinear solution consists of a quasi-stationary part to satisfy the inhomogeneous boundary conditions due to the vessel's motion and a dynamic part which is decomposed into mode shapes. In this paper, alternatively, the dynamic deflections are split into a linear and a modally decomposed nonlinear part. Like *Gardner and Kotch (1976)* for risers, Bliek and Triantafillou solve the nonlinear cable problem by considering all nonlinearities as an initially unknown load to be improved iteratively.

Several practical aspects of offshore pipelaying are discussed by the following two papers.

Based on large deflection beam theory, *Clauss et al. (1977)* published a static analysis of pipe geometry and stresses during laying. Further, a procedure for pipe dimensioning is presented considering the combined stress associated with external pressure and bending moment under laying conditions, allowing for initial out-of-roundness of the pipe.

The most comprehensive variety of practical pipelaying aspects is discussed by *Langner and Ayers (1985)*. They cover technical and economical implications of different laying procedures and discuss how to use the tensioner to avoid prohibitive dynamic tension forces or relative axial motions between pipe and ship.

Many publications deal with the analysis of free pipeline spans on the soil due to scour effects, e.g. *Bruschi et al. (1987)* and *Hobbs (1986)*. This problem is mathematically quite different from pipelaying, but the boundary conditions at the sea floor may be useful also for pipelaying analysis.

This paper presents a unique approach to statics and dynamics of pipelines during laying. It is based on the theory presented by *Weede (1990)* and includes the nonlinear interaction between tension and bending oscillations as well as a sophisticated tensioner control. The results are composed from a frequency domain approach and a modally decomposed improvement in time domain. The theory is validated experimentally. The model testing technique, initially proposed by *Clauss and Kruppa (1974)* and substantially improved since then, achieves model similarity by defining characteristic numbers derived from the non-dimensional differential equations of pipeline dynamics. Comparisons of calculated and measured motions, stresses and loads of typical pipelines prove the reliability of the proposed calculation method.

Symbols

$b(s,t)$ damping parameter
$\tilde{b}(s)$ linearized damping parameter
c_a Morison's added mass coefficient = 1
c_d Morison's drag coefficient
c_{jj} square of the 1st derivative of the j-th normalized mode shape, integrated over the length
D largest diameter, diameter of concrete hull
D_{se} external diameter of steel pipe
d vertical distance from seabed to top of stinger circle (S-method) or to the clamped end (J-method)
E Young's modulus
EI flexural rigidity of steel pipe
EA axial rigidity of steel pipe
$\underline{e}_x, \underline{e}_y, \underline{e}_z$ cartesian vector base in the static touch-down point on the seabed: x=ahead, y=port, z=up
$\underline{e}_S(s), \underline{e}_N(s), \underline{e}_B(s)$ modified moving trihedral of the planar static elastic line: S=tangent, N=lateral in the static plane, B=lateral perpendicular to the static plane
$F_s(s,t)$ effective tension force = real tension force + displacing cross sectional area times external hydrostatic pressure
$F_{sst}(s)$ static part of effective tension force
$F_{sdy}(t)$ dynamic part of effective or real tension force
F_{sj} j-th complex Fourier coefficient of the linearized dynamic tension force $F_0(t)$
$F_0(t)$ linear part of dynamic tension force $F_{sdy}(t)$
$F_1(t)$ nonlinear part of dynamic tension force $F_{sdy}(t)$
g gravity acceleration = $9.81 m/s^2$
H static horizontal effective internal force
k on the soil: beam subgrade modulus; in the free span: zero
L unsupported length
$M_T(s,t)$ torque
$M_{Tj}(s)$ j-th complex Fourier coefficient of torque
m mass per length of pipe plus added mass from water or soil, respectively
m_0 mass per length of the pipe only
$p_N(s,t)$ hydrodynamic lateral line load component from waves and current in the static plane
$p_B(s,t)$ like p_N, but perpendicular to the static plane
$p_{Nj}(s)$ j-th complex Fourier coefficient of the hydrodynamic line load component p_N
$p_{Bj}(s)$ like p_{Nj}, but perpendicular to the static plane
R stinger radius
$T_{Bj}(t)$ like T_{Nj}, but perpendicular to the static plane
$u_j(s)$ j-th normalized mode shape
$u_N(s,t)$ dynamic bending deflections in the static plane
$u_B(s,t)$ dynamic bending deflections perpendicular to the static plane
$u_{Nj}(s)$ j-th complex Fourier coefficient of the linearized bending deflections in the static plane
$u_{Bj}(s)$ like u_{Nj}, but perpendicular to the static plane
$u_{Nj}^{(0)}(s)$ contribution to u_{Nj} from lateral loads and boundary conditions;
$u_{Nj}^{(1)}(s)$ the contribution to u_{Nj} from dynamic tension force is $F_{sj} u_{Nj}^{(1)}$
$u_S(s,t)$ axial dynamic deflection
$u_{SL}(t)$ boundary value of u_S at upper end of unsupported span
$\Delta u_s(t)$ axial pipe motion relative to the vessel
$u_{0N}(s,t)$ linear part of the dynamic bending deflections in the static plane
$u_{0B}(s,t)$ linear part of the dynamic bending deflections perpendicular to the static plane
$u_{1N}(s,t)$ nonlinear part of the dynamic bending deflections in the static plane
$u_{1B}(s,t)$ nonlinear part of the dynamic bending deflections perpendicular to the static plane
V static bottom support force
$v_N(s,t)$ external flow velocity lateral to the pipe in the static plane
$v_B(s,t)$ external flow velocity lateral to the pipe perpendicular to the static plane
w submerged weight per length (weight in air minus buoyancy)
$x_{st}(s)$ horiz. component of planar static elastic line
$z_{st}(s)$ vertical component of planar static elastic line

β parameter of the Newmark method; e.g.: 0.25
$\beta_{ik}(t)$ damping parameter times i-th times k-th normalized mode shape, integrated over the length
$\tilde{\beta}_{ik}$ linear part of β_{ik}
$\Delta\beta_{jj}(t)$ nonlinear part of β_{jj}
κ_j j-th modal coefficient of $\varphi'(s)$
μ_{jj} mass distribution m times square of j-th normalized mode shape, integrated over the lenght
ϱ specific mass of sea water = $1025\ kg/m^3$
$\tau_{Nj}(t)$ j-th modal coefficient of the nonlinear part of the bending deflection in the static plane
$\tau_{Bj}(t)$ like τ_{Nj}, but perpendicular to the static plane

$\underline{r}(s,t)$	radius vector of pipe axis from static touch-down point	$\varphi(s)$	static inclination angle
		$\|\varphi'(s)\|$	static curvature
s	curve length from static touch-down point, upwards positive	Ω_j	j-th natural circular frequency
		ω	circular frequency
t	time		
$T_{Nj}(t)$	j-th modal coefficient of the linearized dyn. bending deflection in the static plane	$()'$	$\partial/\partial s$
		$(\dot{})$	$\partial/\partial t$
		$()_L$	boundary value at top of free span

2. Basic Equations

The configuration of the pipeline as a Bernoulli beam is defined by the radius vector $\underline{r}(s,t)$ of the pipe axis and the torsional angle $\chi(s,t)$ as functions of curve length s and time t. Partial derivatives will be designated by $()' = \partial/\partial s$ and $(\dot{}) = \partial/\partial t$.

The pipe has the mass per length m_0 and the torsional mass moment of inertia per length Θ. We regard a pipe element, length ds, loaded by an external line load $\underline{q}$ and internal forces $\underline{F}$ and moments $\underline{M}$ at both ends.

As the hydrostatic pressure is only acting on the wetted surface, the resulting force is normal to the pipe axis. It is easier, however, to substitute this force by
- a vertical buoyancy force which results from the pressure effect on the wetted surface and the non-wetted cross sections, and – for appropriate correction –
- axial tension forces which result from the negative external hydrostatic pressure acting on the non-wetted cross sections.

The vertical buoyancy contributes to the external line load vector $\underline{q}$, and the correcting axial tension forces are added to the internal force vector, i.e. the resultant "effective" internal force $\underline{F}$ consists not only of the stress relevant forces, but also of these axial hydrostatic force corrections.

The basic equations are derived from the dynamic force equilibrium, from the dynamic moment equilibrium neglecting bending rotatory inertia according to Bernoulli beam theory and from the constitutive equations of bending and torsion of circular pipes. Table 1 shows the derivation of the basic equations similar to a flow chart.

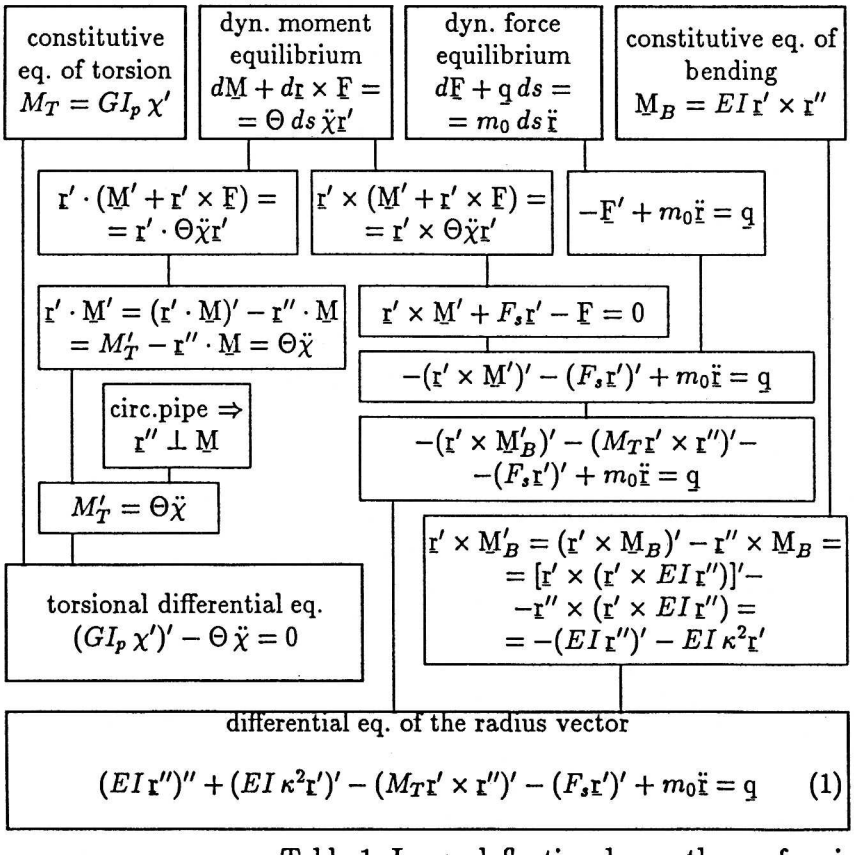

Table 1: Large deflection beam theory for circular pipes

The configuration $\underline{r}(s,t)$ of the pipeline is split into a planar static configuration $\underline{r}_{st}(s)$ and a dynamic deflection $\underline{u}(s,t)$. The planar static load only consists of the submerged weight per unit length (reduced by buoyancy): $\underline{q}_{st} = -w\underline{e}_z$. The planar static configuration $\underline{r}_{st}(s)$ can be defined by its inclination angle $\varphi(s)$ versus the horizontal direction.

With the moving trihedral – see Fig.1 –

$$\underline{e}_S = \cos\varphi\,\underline{e}_x + \sin\varphi\,\underline{e}_z = \underline{r}'_{st} \qquad \underline{e}_N = -\sin\varphi\,\underline{e}_x + \cos\varphi\,\underline{e}_z = \underline{r}''_{st}/\varphi' \qquad \underline{e}_B = -\underline{e}_y$$

the planar static configuration is calculated by integrating Eq. (1) and substituting $\underline{r}'_{st} = \underline{e}_S$ and $\underline{r}''_{st} = \varphi'\underline{e}_N$. With constant EI this results in the vector equation

$$EI\,\varphi''\underline{e}_N - F_{sst}\,\underline{e}_S = -H\underline{e}_x - (ws - V)\underline{e}_z$$

The integration constants are the effective horizontal force H and the bottom support force V. The lateral and axial component equations define the static problem:

$$EI\,\varphi''(s) - H\sin\varphi(s) + (ws - V)\cos\varphi(s) = 0 \tag{2}$$

$$\underline{r}_{st}(s) = \int \cos\varphi(s)\,ds\,\underline{e}_x + \int \sin\varphi(s)\,ds\,\underline{e}_z$$

$$F_{sst}(s) = H\cos\varphi(s) + (ws - V)\sin\varphi(s) \tag{3}$$

The nonlinear differential equation (2) is solved to obtain the static curvature $|\varphi'(s)|$ and effective tension force $F_{sst}(s)$ for stress calculation and the static configuration $\underline{r}_{st}(s)$. $F_{sst}(s)$ and $\varphi'(s)$ also have a significant influence on the dynamic response.

The dynamic configuration is also calculated from Eq. (1) after splitting off the static terms. As specified by *Weede (1990)*, uncoupling is achieved by approximating the derivatives $\underline{u}'$ and $\underline{u}''$ of the dynamic deflection vector. The dynamic lateral deflections in the static bending plane (N) and perpendicular to it (B) are calculated from the component equations

$$EI\,u''''_N - (F_s u'_N)' + m_0\ddot{u}_N = \varphi' F_{sdy} + q_{Ndy} \tag{4}$$

$$EI\,u''''_B - (F_s u'_B)' + m_0\ddot{u}_B = (\varphi' M_T)' + q_{Bdy} \tag{5}$$

On the left-hand side, the dynamic tension force F_{sdy} contributes to the effective tension force $F_s = F_{sst} + F_{sdy}$ introducing a time-dependent stiffness. On the right-hand side, it yields a pseudo line load in combination with the static curvature. As $F_{sdy} = EA\epsilon_{dy}$ it depends on the dynamic strain

$$\epsilon_{dy} \approx u'_S - \varphi' u_N + \frac{u'^2_N}{2} + \frac{u'^2_B}{2} \tag{6}$$

which is a function of axial motions u_S and lateral motions u_N, u_B *(Weede 1990)*. The two squared terms reflect that the dynamic shape requires more curve length than the static configuration; this phenomenon stiffens the pipeline by increasing the mean dynamic tension. The additional term $\varphi' u_N$ illustrates the fact that axial and lateral deflections are coupled at large static curvature φ'.

Axial elastic vibrations are neglected, as the first axial natural frequency is too high to be excited by the seaway. Consequently, the dynamic tension force has nearly the same amplitude and phase all along the pipe (Kirchhoff's hypothesis, *Kauderer 1958*) and may be averaged over the unsupported span:

$$F_{sdy} \approx \frac{1}{L}\int_{(L)} F_{sdy}\,ds = \frac{EA}{L}\int_{(L)} \epsilon_{dy}\,ds \tag{7}$$

The hydrodynamic load components in the unsupported span, q_{Ndy} and q_{Bdy}, are deduced from the generalized Morison equation (see *Clauss et al. 1988*). In the planar case, where the pipe moves with the lateral deflection u, and the external flow velocity from waves and current has the lateral component v, it yields:

$$q_{dy} - m_0\ddot{u} = \underbrace{(1+c_a)\varrho\frac{\pi D^2}{4}\dot{\mathrm{v}} + \underbrace{c_d\frac{\varrho}{2}D|\dot{u}-\mathrm{v}|}_{b(s,t)}\mathrm{v}}_{p(s,t)} - \underbrace{(m_0+c_a\varrho\frac{\pi D^2}{4})}_{m}\ddot{u} - \underbrace{c_d\frac{\varrho}{2}D|\dot{u}-\mathrm{v}|}_{b(s,t)}\dot{u} \tag{8}$$

where m is the effective mass per unit length, $b(s,t)$ is the damping parameter and $p(s,t)$ is the load contribution from waves and current. The added mass coefficient of a circular cylinder is $c_a = 1$, and for the drag coefficient we propose $c_d = 1.2$.

Beyond the touch-down point, the pipe on the sea floor is treated as a generalized Winkler beam with linear elasticity, damping and inertia forces. At some distance from the touch-down point a clamped end is assumed.

A three-dimensional generalization of Eq. (8) is introduced into Eqs. (4) and (5) for the free span. For the span laying on the ground, the soil mechanical equivalent is taken. Eq. (6) is introduced into Eq. (7). Thus, the dynamic problem consists of two differential equations of bending oscillations in the static plane (N) and perpendicular to it (B) and of the averaged axial constitutive equation specifying the dynamic tension force:

$$EI\,u_N'''' - (F_s u_N')' + ku_N + m\ddot{u}_N + b\dot{u}_N = \varphi' F_{sdy} + p_N \tag{9}$$

$$EI\,u_B'''' - (F_s u_B')' + ku_B + m\ddot{u}_B + b\dot{u}_B = (\varphi' M_T)' + p_B \tag{10}$$

$$F_{sdy} = \frac{EA}{L}\left[u_{sL} - \int_{(L)}\left(\varphi' u_N - \frac{u_N'^2}{2} - \frac{u_B'^2}{2}\right)ds\right] \tag{11}$$

In the unsupported span the parameters are:

$$k = 0 \qquad m = m_0 + c_a\varrho\frac{\pi D^2}{4} \qquad b = c_d\frac{\varrho}{2}D\sqrt{(\dot{u}_N-\mathrm{v}_N)^2 + (\dot{u}_B-\mathrm{v}_B)^2} \tag{12}$$

$$p_N = (1+c_a)\varrho\frac{\pi D^2}{4}\dot{\mathrm{v}}_N + b\mathrm{v}_N \qquad p_B = (1+c_a)\varrho\frac{\pi D^2}{4}\dot{\mathrm{v}}_B + b\mathrm{v}_B$$

On the seabed, the influence of the loads p_N and $p_B = 0$ may be neglected and k (beam subgrade modulus), m (pipe mass plus soil added mass per unit lenght) and b (soil damping) are determined from linearized soil mechanics.

The axial pipe deflection relative to the vessel (inside the welding station) follows from the axial motion of the pipe head $u_{sL}(t) = u_s(s=L,t)$ and the associated vessel motion component $u_v(t)$:

$$\Delta u_s(t) = u_{sL}(t) - u_v(t) \tag{13}$$

If the tensioner is blocked, this relative axial deflection is zero, the dynamic tension force $F_{sdy}(t)$ is unknown and Eq. (11) is coupled with Eqs. (9) and (10). If the resulting dynamic tension force threatens to leave a permissible range, the tensioner drive will start to compensate as long as necessary, keeping F_{sdy} on the upper or lower limit. During compensation, Eqs. (9) and (10) are solved with the known F_{sdy} and Eq. (11) is resolved with respect to the axial pipe head motion $u_{sL}(t)$ to obtain the relative axial motion $\Delta u_s(t)$ from Eq. (13). Thus, a very large permissible range results in a permanently blocked tensioner, and a zero sized permissible range results in a permanently compensating tensioner. Only these two cases can be considered in the frequency domain approach.

3. Planar Static Solution

As specified in the basic equations, the pipeline configuration $\underline{r}(s,t)$ is composed of a planar static elastic line $\underline{r}_{st}(s)$ and a dynamic deflection $\underline{u}(s,t)$. The static inclination angle $\varphi(s)$ and the resulting pipeline configuration are calculated by solving Eq. (2). Static bending stresses $\sigma_B = \pm E\varphi' D_{se}/2$ depend on φ' (curvature $\kappa_{st} = |\varphi'|$) which also is an important term for the dynamic analysis. The static effective tension force F_{sst} follows from Eq. (3). Note that for stress calculations the effective tension force has to be reduced by the hydrostatic pressure contribution $\varrho g(d_0 - z_{st})\frac{\pi D^2}{4}$ as the cross sections of the pipe element are non wetted. $(d_0 - z_{st})$ is the element depth below the water surface. For solving Eqs. (2) and (3) a numerical solution was selected. Further, for speeding up the calculations, the following analytical approach was developed *(Weede 1990)*, based on an approximate solution $\varphi(s)$ of Eq. (2).

Inclination angle $\varphi(s)$:

$$\varphi(s) = \arctan\left(\frac{\mathrm{w}s - V}{H}\right) + \sqrt{\frac{EI\,\mathrm{w}^2}{H^3}}\left[\left(\frac{H\varphi'_L}{\mathrm{w}} - \frac{1}{1+\left(\frac{\mathrm{w}L-V}{H}\right)^2}\right)\frac{\mathrm{ch}\left(s\sqrt{\frac{H}{EI}}\right)}{\mathrm{sh}\left(L\sqrt{\frac{H}{EI}}\right)} + \frac{1}{1+\left(\frac{V}{H}\right)^2}\frac{\mathrm{ch}\left((L-s)\sqrt{\frac{H}{EI}}\right)}{\mathrm{sh}\left(L\sqrt{\frac{H}{EI}}\right)}\right]$$

Curvature $|\varphi'(s)|$:

$$\frac{H\varphi'(s)}{\mathrm{w}} = \frac{1}{1+\left(\frac{\mathrm{w}s-V}{H}\right)^2} + \left(\frac{H\varphi'_L}{\mathrm{w}} - \frac{1}{1+\left(\frac{\mathrm{w}L-V}{H}\right)^2}\right)\frac{\mathrm{sh}\left(s\sqrt{\frac{H}{EI}}\right)}{\mathrm{sh}\left(L\sqrt{\frac{H}{EI}}\right)} - \frac{1}{1+\left(\frac{V}{H}\right)^2}\frac{\mathrm{sh}\left((L-s)\sqrt{\frac{H}{EI}}\right)}{\mathrm{sh}\left(L\sqrt{\frac{H}{EI}}\right)}$$

Pipe geometry $x_{st}(s), z_{st}(s)$:

$$x_{st}(s) = \int_0^s \cos\varphi(s)ds \qquad z_{st}(s) = \int_0^s \sin\varphi(s)ds$$

Effective tension force $F_{sst}(s)$:

$$F_{sst}(s) = H\cos\varphi(s) + (\mathrm{w}s - V)\sin\varphi(s) \quad \approx \quad H\sqrt{1+\left(\frac{\mathrm{w}s-V}{H}\right)^2}$$

Bottom support force V:

$$\frac{V}{H} \approx \sqrt[3]{\sqrt{\frac{EI\,\mathrm{w}^2}{4H^3} + \frac{1}{27}} + \sqrt{\frac{EI\,\mathrm{w}^2}{4H^3}}} - \sqrt[3]{\sqrt{\frac{EI\,\mathrm{w}^2}{4H^3} + \frac{1}{27}} - \sqrt{\frac{EI\,\mathrm{w}^2}{4H^3}}}$$

The equations are evaluated using known values for:

- w submerged weight per unit length
- EI flexural rigidity
- d depth from seabed to the horizontal tensioner axis (see Fig.1) in case of S-method or to the clamped end in case of J-method
- H horizontal force
- φ'_L boundary curvature at upper end of the unsupported span.
  J-method: $\varphi'_L = 0$; S-method: $\varphi'_L = -1/R$, where R = stinger radius.

The exact bottom support force (the above expression is an approximation only) is determined iteratively from the condition $\varphi(0) = 0$. The unsupported length L is obtained via a binary search from the boundary condition

$$z_{st}(s=L) = \begin{cases} d - R(1-\cos\varphi(s=L)) & \text{in case of S-method} \\ d & \text{in case of J-method} \end{cases}$$

4. Linearized Dynamic Solution

The dynamic deflections and tension force are calculated from Eqs. (9)-(11). Linearization consists of four assumptions:

- The total effective tension force $F_s(s,t)$ on the left side of Eqs. (9) and (10) is approximated by its static value $F_{sst}(s)$;
- the square strain terms in Eq. (11) are neglected;
- for the hydrodynamic damping parameter $b(s,t)$ a time independent approximation $\tilde{b}(s)$ is taken and improved iteratively to minimize the square error of the drag force.
- The tensioner is either permanently blocked (F_{sdy} unknown, $\Delta u_s = 0$) or permanently compensating ($F_{sdy} = 0$, Δu_s unknown).

Using these assumptions, Eqs. (9), (10) and (11) as well as the dynamic boundary conditions, i.e. the vessel motions, are converted to frequency domain by taking their Fourier transform using the general definitions

$$f(t) = \sum_{j=-n}^{n} f_j \, e^{i\omega_j t} \; ; \qquad f_j = \frac{1}{T} \int_{(T)} f(t) \, e^{-i\omega_j t} \, dt \; .$$

where f_j are the complex Fourier coefficients and $\omega_j = 2\pi j/T$ are the circular frequencies with T being a sufficiently large time window.

The Fourier transform of Eq. (9) cannot be solved directly if the tensioner is blocked, as on its right-hand side the complex Fourier coefficients F_{sj} of the dynamic tension force are unknown in this case. Therefore, the complex Fourier coefficients of the linearized bending deflections in the N-direction are split into contributions i) from lateral loads and boundary conditions, and ii) from dynamic tension force:

$$u_{Nj} = u_{Nj}^{(0)} + F_{sj} u_{Nj}^{(1)} \tag{14}$$

Introducing this into the Fourier transform of Eq. (9) produces two equations which now can be solved as their right-hand sides are known, i.e. the complex Fourier coefficients of the wave and current loads p_{Nj} in the equation for $u_{Nj}^{(0)}$ and the static curvature φ' in the equation for $u_{Nj}^{(1)}$. The solution has to comply with the boundary conditions, as imposed by the vessel motions in the seaway. If this is considered in $u_{Nj}^{(0)}$, the boundary values of $u_{Nj}^{(1)}$ must be zero.

Eq. (14) is substituted into the Fourier transform of Eq. (11) neglecting the squared terms:

$$F_{sj} = \frac{EA}{L} \left[u_{sLj} - \int_{(L)} \varphi' \left(u_{Nj}^{(0)} + F_{sj} u_{Nj}^{(1)} \right) ds \right]$$

and this is resolved with respect to the complex Fourier coefficients F_{sj} of the dynamic tension force.

The linear dynamic differential equations of the pipe bending deflections, used for the numerical solution, are summarized as follows:

$$EI u_{Nj}^{(0)\,\prime\prime\prime\prime} - (F_{sst} u_{Nj}^{(0)\,\prime})' + (k - \omega_j^2 m + i\omega_j \tilde{b}) u_{Nj}^{(0)} = p_{Nj} \qquad \text{inhomogeneous boundary conditions: vessel motion} \tag{15}$$

$$EI u_{Nj}^{(1)\,\prime\prime\prime\prime} - (F_{sst} u_{Nj}^{(1)\,\prime})' + (k - \omega_j^2 m + i\omega_j \tilde{b}) u_{Nj}^{(1)} = \varphi' \qquad \text{homogeneous boundary conditions: all zero} \tag{16}$$

$$EI u_{Bj}'''' - (F_{sst} u_{Bj}')' + (k - \omega_j^2 m + i\omega_j \tilde{b}) u_{Bj} = (\varphi' M_{Tj})' + p_{Bj} \qquad \text{inhomogeneous boundary conditions: vessel motion} \tag{17}$$

$$F_{sj} = \frac{u_{sLj} - \int\limits_{(L)} \varphi' u_{Nj}^{(0)}\, ds}{\frac{L}{EA} + \int\limits_{(L)} \varphi' u_{Nj}^{(1)}\, ds} \tag{18}$$

$$u_{Nj} = u_{Nj}^{(0)} + F_{sj}\, u_{Nj}^{(1)}$$

Eqs. (16) and (18) have to be evaluated only if the tensioner is blocked. In the opposite case, if the tensioner is compensating, the F_{sj} are zero and Eq. (18) is resolved with respect to the complex Fourier coefficients u_{sLj} of the axial pipe head motion in order to obtain the pipe axial motion relative to the vessel from Eq. (13). The $u_{Nj}^{(1)}$ are not required in case of compensating tensioner.

The numerical solution is embedded in two nested loops. The internal loop steps along the circular frequencies ω_j, whereas the external one serves to improve the linearized damping parameter iteratively:

$$\tilde{b}(s) = c_d \frac{\varrho}{2} D \frac{\int\limits_{(T)} \left[(\dot{u}_N - v_N)^2 + (\dot{u}_B - v_B)^2\right]^{3/2} dt}{\int\limits_{(T)} \left[(\dot{u}_N - v_N)^2 + (\dot{u}_B - v_B)^2\right] dt} \tag{19}$$

Eqs. (15), (16) and (17) are linear inhomogeneous ordinary differential equations with variable complex coefficients. For solving this kind of equations, an algorithm was implemented which accepts a wide variety of inhomogeneous boundary and intermediate conditions *(Weede 1990)*. It is based on the Galerkin finite element method and uses deflection and inclination at the nodes as unknowns.

5. Nonlinear Dynamic Correction

Model tests have shown that the dynamic response to a harmonic excitation contains components at integer multiples and integer fractures of the excitation frequency. In comparison to the component at the excitation frequency itself, their amplitudes may not be neglected at higher frequencies (see Fig. 5). For this reason a nonlinear correction is added to the linearized dynamic bending deflections and tension force.

The following nonlinearities are analyzed:

- The total effective tension force $F_s(s,t)$ on the left hand side of Eqs. (9) and (10) provides a time-dependent stiffness.
- According to Eqs. (9)–(11), the dynamic bending deflections and tension force mutually depend on each other if the tensioner is blocked, and the square terms in Eq. (11) make this dependency nonlinear.
- The hydrodynamic drag load yields a nonlinear behaviour.

At the lift-off point on the stinger, the total bending deflections must be equal to the given vessel motions. As the linearized solution already satisfies this condition, the nonlinear correction must be zero there. This allows to compose the nonlinear correction of individual mode shapes.

The bending deflections and the parameters are split into linear and nonlinear parts:

total = linear + nonlinear
$u_N(s,t) = u_{0N}(s,t) + u_{1N}(s,t)$ = dyn.bending deflections (N)
$u_B(s,t) = u_{0B}(s,t) + u_{1B}(s,t)$ = dyn.bending deflections (B)
$F_{sdy}(t) = F_0(t) + F_1(t)$ = dyn.tension force
$b(s,t) = \tilde{b}(s) + \Delta b(s,t)$ = damping parameter
$\Delta u_s(t) = \Delta u_{s0}(t) + \Delta u_{s1}(t)$ = axial pipe deflection relative to the vessel

Eqs. (9) and (10) are decomposed accordingly. Their nonlinear part is split off as follows:

$$EIu''''_{1N}-(F_{sst}u'_{1N})'-F_{sdy}(u''_{0N}+u''_{1N})+ku_{1N}+m\ddot{u}_{1N}+b\dot{u}_{1N}+\Delta b\dot{u}_{0N} = \varphi' F_1 \qquad (20)$$

$$EIu''''_{1B}-(F_{sst}u'_{1B})'-F_{sdy}(u''_{0B}+u''_{1B})+ku_{1B}+m\ddot{u}_{1B}+b\dot{u}_{1B}+\Delta b\dot{u}_{0B} = 0 \qquad (21)$$

Note that $F_s(s,t) = F_{sst}(s) + F_{sdy}(t)$.

The linear and the nonlinear part of the dynamic bending deflections are decomposed into mode shapes:

$$u_{0N}(s,t) = \sum_{(j)} u_j(s) T_{Nj}(t) \qquad u_{0B}(s,t) = \sum_{(j)} u_j(s) T_{Bj}(t) \qquad (22)$$

$$u_{1N}(s,t) = \sum_{(j)} u_j(s) \tau_{Nj}(t) \qquad u_{1B}(s,t) = \sum_{(j)} u_j(s) \tau_{Bj}(t) \qquad (23)$$

where the $\tau_{Nj}(t), \tau_{Bj}(t)$ are unknown and the $T_{Nj}(t), T_{Bj}(t)$ follow from the linear solution:

$$T_{Nj}(t) = \int_{(L)} u_j(s)\, u_{0N}(s,t)\, dt \qquad T_{Bj}(t) = \int_{(L)} u_j(s)\, u_{0B}(s,t)\, dt$$

The mode shapes $u_j(s)$ and the associated natural frequencies Ω_j follow from

$$EI\, u_j'''' - (F_{sst} u_j)' + k\, u_j - \Omega_j^2 m\, u_j = 0 \qquad \text{where} \int_{(L)} u_j\, u_k\, ds = \delta_{jk} = \begin{cases} 1 \text{ if } j = k \\ 0 \text{ else} \end{cases} \qquad (24)$$

Introducing the modal decompositions (22) and (23) into Eqs. (20) and (21) yields

$$\sum_{(j)} \left[(m\ddot{\tau}_{Nj} + b\dot{\tau}_{Nj}) u_j + \left(EI\, u_j'''' - (F_{sst} u_j')' + k u_j \right) \tau_{Nj} - F_{sdy} u_j'' \tau_{Nj} \right] = \sum_{(j)} \left[F_{sdy} u_j'' T_{Nj} - \Delta b u_j \dot{T}_{Nj} \right] + \varphi' F_1 \qquad (25)$$

$$\sum_{(j)} \left[(m\ddot{\tau}_{Bj} + b\dot{\tau}_{Bj}) u_j + \left(EI\, u_j'''' - (F_{sst} u_j')' + k u_j \right) \tau_{Bj} - F_{sdy} u_j'' \tau_{Bj} \right] = \sum_{(j)} \left[F_{sdy} u_j'' T_{Bj} - \Delta b u_j \dot{T}_{Bj} \right] \qquad (26)$$

Eq. (24) allows to substitute $EI\, u_j'''' - (F_{sst} u_j)' + k\, u_j$ by $\Omega_j^2 m u_j$. Eqs. (25) and (26) are now multiplied by $u_i(s)$ and integrated over the pipe length. This is abbreviated as follows:

$$\sum_{(j)} \left[\mu_{ij} \ddot{\tau}_{Nj} + \beta_{ij} \dot{\tau}_{Nj} + (\Omega_j^2 \mu_{ij} + F_{sdy} c_{ij}) \tau_{Nj} \right] = \sum_{(j)} \left[-F_{sdy} c_{ij} T_{Nj} - \Delta \beta_{ij} \dot{T}_{Nj} \right] + F_1 \kappa_i$$

$$\sum_{(j)} \left[\mu_{ij} \ddot{\tau}_{Bj} + \beta_{ij} \dot{\tau}_{Bj} + (\Omega_j^2 \mu_{ij} + F_{sdy} c_{ij}) \tau_{Bj} \right] = \sum_{(j)} \left[-F_{sdy} c_{ij} T_{Bj} - \Delta \beta_{ij} \dot{T}_{Bj} \right]$$

Thus, two partial differential equations for $u_{1N}(s,t), u_{1B}(s,t)$ have been transformed into two systems of ordinary differential equations for $\tau_{Nj}(t), \tau_{Bj}(t)$. Their coefficients are specified as follows:

$$\mu_{ij} = \int_{(L)} u_i m u_j ds \qquad c_{ij} = -\int_{(L)} u_i u_j'' ds = \int_{(L)} u_i' u_j' ds \qquad \kappa_i = \int_{(L)} u_i \varphi' ds \qquad (27)$$

$$\tilde{\beta}_{ij} = \int_{(L)} u_i \tilde{b} u_j ds \qquad \Delta\beta_{ij} = \int_{(L)} u_i \Delta b u_j ds \qquad \beta_{ij} = \int_{(L)} u_i b u_j ds = \tilde{\beta}_{ij} + \Delta\beta_{ij} \qquad (28)$$

As the mode shapes are orthogonal with respect to to the mass distribution, the inertia terms are uncoupled: $\mu_{ij} = 0$ if $i \neq j$. Approximately, the first derivatives of the mode shapes are orthogonal to each other, i.e. $c_{ij} \ll c_{ii}$ if $i \neq j$. It is common practice in modal analysis to assume that the

mode shapes are approximately orthogonal with respect to the damping distribution $b(s,t)$, i.e. to assume that $|\beta_{ij}| \ll |\beta_{ii}|$ if $i \neq j$. In case of offshore pipelaying, however, the damping parameter is strongly variable along the pipe, and this assumption becomes rather unexact. It is better to uncouple only the relatively small nonlinear part, i.e. $|\Delta\beta_{ij}| \ll |\Delta\beta_{ii}|$ if $i \neq j$. From the linear part $\tilde{\beta}_{ij}$, the members $i \neq j$ are neglected only initially and taken into account by means of an iterative improvement.

With these uncouplings, the two ordinary differential equation systems are

$$\mu_{ii}\ddot{\tau}_{Ni} + \beta_{ii}\dot{\tau}_{Ni} + (\Omega_i^2\mu_{ii} + F_{sdy}c_{ii})\tau_{Ni} = -F_{sdy}c_{ii}T_{Ni} - \Delta\beta_{ii}\dot{T}_{Ni} + F_1\kappa_i - \sum_{(j\neq i)} \tilde{\beta}_{ij}\dot{\tau}_{Nj} \quad (29)$$

$$\mu_{ii}\ddot{\tau}_{Bi} + \beta_{ii}\dot{\tau}_{Bi} + (\Omega_i^2\mu_{ii} + F_{sdy}c_{ii})\tau_{Bi} = -F_{sdy}c_{ii}T_{Bi} - \Delta\beta_{ii}\dot{T}_{Bi} - \sum_{(j\neq i)} \tilde{\beta}_{ij}\dot{\tau}_{Bj} \quad (30)$$

Eqs. (29) and (30) are solved by the Newmark method, as described by *Burnett (1987)*. It is a method to solve differential equations of motion with an algorithm which steps along time t with a constant timestep Δt. At each timestep the unknown velocities $\dot{f}(t)$ and accelerations $\ddot{f}(t)$ are expressed by the unknown deflections $f(t)$ and by the known results $f(t-\Delta t), \dot{f}(t-\Delta t), \ddot{f}(t-\Delta t)$ from the previous timestep. $f(t)$ represents either a function of one or more coordinates or a vector (one-column matrix) holding the discrete motions of a finite-element system. To substitute unknown velocities and accelerations, the Newmark method uses a modified Taylor expansion of the deflections and velocities:

$$\left.\begin{aligned} f(t) &\approx f(t-\Delta t) + \Delta t\dot{f}(t-\Delta t) + \frac{\Delta t^2}{2}\left((1-2\beta)\ddot{f}(t-\Delta t) + 2\beta\ddot{f}(t)\right) \\ \dot{f}(t) &\approx \dot{f}(t-\Delta t) + \Delta t\left((1-\gamma)\ddot{f}(t-\Delta t) + \gamma\ddot{f}(t)\right) \end{aligned}\right\} \Rightarrow$$

$$\Rightarrow \left\{\begin{aligned} \dot{f}(t) &\approx (f(t)-f(t-\Delta t))\frac{\gamma}{\beta\Delta t} - \dot{f}(t-\Delta t)\left(\frac{\gamma}{\beta}-1\right) - \ddot{f}(t-\Delta t)\left(\frac{\gamma}{2\beta}-1\right)\Delta t \\ \ddot{f}(t) &\approx (f(t)-f(t-\Delta t))\frac{1}{\beta\Delta t^2} - \dot{f}(t-\Delta t)\frac{1}{\beta\Delta t} - \ddot{f}(t-\Delta t)\left(\frac{1}{2\beta}-1\right) \end{aligned}\right.$$

For the coefficients β and γ we recommend $\beta = 0.25, \gamma = 0.5$; for details see *Burnett (1987)*. The Newmark method may be abbreviated as

$$\dot{f} \approx (f-f^*)\alpha_{10} - \dot{f}^*\alpha_{11} - \ddot{f}^*\alpha_{12}\,; \qquad \ddot{f} \approx (f-f^*)\alpha_{20} - \dot{f}^*\alpha_{21} - \ddot{f}^*\alpha_{22} \quad (31)$$

where magnitudes related to the previous timestep are marked with an $()^*$, e.g. $f = f(t), f^* = f(t-\Delta t)$, and the following abbreviations are defined:

$$\alpha_{10} = \frac{\gamma}{\beta}/\Delta t \qquad \alpha_{11} = \frac{\gamma}{\beta} - 1 \qquad \alpha_{12} = \left(\frac{\gamma}{2\beta} - 1\right)\Delta t \quad (32)$$

$$\alpha_{20} = \frac{1}{\beta}/\Delta t^2 \qquad \alpha_{21} = \frac{1}{\beta}/\Delta t \qquad \alpha_{22} = \frac{1}{2\beta} - 1 \quad (33)$$

Applying Eq. (31) to Eqs. (29) and (30), they can be resolved with respect to the deflections at the current timestep:

$$\tau_{Ni} = \frac{(\kappa_i - c_{ii})F_{sdy} + \mu_{ii}(\alpha_{20}\tau^*_{Ni} + \alpha_{21}\dot{\tau}^*_{Ni} + \alpha_{22}\ddot{\tau}^*_{Ni}) + \beta_{ii}(\alpha_{10}\tau^*_{Ni} + \alpha_{11}\dot{\tau}^*_{Ni} + \alpha_{12}\ddot{\tau}^*_{Ni})}{c_{ii}F_{sdy} + (\Omega_i^2 + \alpha_{20})\mu_{ii} + \alpha_{10}\beta_{ii}} +$$
$$+ \frac{-\Delta\beta_{ii}\dot{T}_{Ni} - F_0\kappa_i - \sum_{(j\neq i)} \tilde{\beta}_{ij}\dot{\tau}_{Nj}}{c_{ii}F_{sdy} + (\Omega_i^2 + \alpha_{20})\mu_{ii} + \alpha_{10}\beta_{ii}} \quad (34)$$

$$\tau_{Bi} = \frac{-c_{ii}F_{sdy} + \mu_{ii}(\alpha_{20}\tau^*_{Bi} + \alpha_{21}\dot{\tau}^*_{Bi} + \alpha_{22}\ddot{\tau}^*_{Bi}) + \beta_{ii}(\alpha_{10}\tau^*_{Bi} + \alpha_{11}\dot{\tau}^*_{Bi} + \alpha_{12}\ddot{\tau}^*_{Bi})}{c_{ii}F_{sdy} + (\Omega_i^2 + \alpha_{20})\mu_{ii} + \alpha_{10}\beta_{ii}} +$$
$$+ \frac{-\Delta\beta_{ii}\dot{T}_{Bi} - \sum_{(j\neq i)} \tilde{\beta}_{ij}\dot{\tau}_{Bj}}{c_{ii}F_{sdy} + (\Omega_i^2 + \alpha_{20})\mu_{ii} + \alpha_{10}\beta_{ii}} \quad (35)$$

The sum expressions are initially omitted and improved iteratively. The $\Delta\beta_{ii}$ require the determination of the velocity-dependent damping parameter, see Eq. (12). For this purpose the velocity is linearly extrapolated from the previous timestep.

The above expressions for τ_{Ni}, τ_{Bi} are functions of the dynamic tension force F_{sdy}. A tensioner control which keeps F_{sdy} within a permissible range is simulated by the following calculation of F_{sdy} at each timestep: An espression for the pipe axial deflection relative to the vessel can be deduced from Eqs. (11) and (13). Splitting off its linear part known from the linear solution and itroducing the modal decompositions into the nonlinear remainder yields

$$\Delta u_s = \Delta u_{s0} + \frac{L}{EA}(F_{sdy} - F_0) + \sum_{(j)} \left[\kappa_j \tau_{Nj} - \frac{c_{jj}}{2}(T_{Nj} + \tau_{Nj})^2 - \frac{c_{jj}}{2}(T_{Bj} + \tau_{Bj})^2 \right] \tag{36}$$

where either $\Delta u_{s0} = 0$ or $F_{s0} = 0$ depending on the tensioner control mode assumed for the previous linear solution.

A binary search for the zero-crossing of this function aims to find the F_{sdy} which causes the tensioner to stop ($\Delta u_s = 0$). As the predefined permissible range is taken as initial search interval, F_{sdy} converges towards
- the F_{sdy} which yields $\Delta u_s = 0$ if acceptable;
- the lower limit if the required F_{sdy} would be too small;
- the upper limit if the required F_{sdy} would be too large.

Thus, both tensioner control modes may alternate in the most general case.

The algorithm of the nonlinear correction follows the subsequent procedure:

Solve linear problem: $u_{0N}, u_{0B}, F_0, \tilde{b}, \Delta u_{s0}$
mode shapes u_j and nat.circ. frequencies Ω_j from Eq. (24).
α_{ij} from Eqs. (32),(33); $\mu_{ii}, c_{ii}, \kappa_i$ and all $\tilde{\beta}_{ij}$ from Eqs. (27) and (28)
initial conditions: $\tau^*_{Ni} = \dot{\tau}^*_{Ni} = \ddot{\tau}^*_{Ni} = \tau^*_{Bi} = \dot{\tau}^*_{Bi} = \ddot{\tau}^*_{Bi} = 0$
loop over the time: $t = 0, \Delta t, 2\Delta t, 3\Delta t, \ldots$
Initially ($t < t_1$) multiply linear results by $3(t/t_1)^2 - 2(t/t_1)^3$
$T_{Ni}, T_{Bi}, \dot{T}_{Ni}, \dot{T}_{Bi}$ from modal decomposition of the linear results
$\Delta\beta_{ii}$ from Eq. (28) with linearly extrapolated velocities
set search interval F_{min}, F_{max} to the given permissible range
$F_{sdy} = (F_{max} + F_{min})/2$
set the sum terms in Eqs. (34),(35) to zero
τ_{Ni}, τ_{Bi} from Eqs. (34), (35).
until the sum terms in Eqs. (34),(35) are good
relative axial deflection Δu_S from Eq. (36).
$\Delta u_S > 0$? — yes: $F_{max} = F_{sdy}$ — no: $F_{min} = F_{sdy}$
until precision of dynamic tension force F_{sdy} is reached
evaluate Eq. (23), superimpose that to linear deflections
velocities $\dot{\tau}_{Ni}, \dot{\tau}_{Bi}$ and accelerations $\ddot{\tau}_{Ni}, \ddot{\tau}_{Bi}$ like Eq. (31)
copy $\tau_{Ni}, \dot{\tau}_{Ni}, \ddot{\tau}_{Ni}, \tau_{Bi}, \dot{\tau}_{Bi}, \ddot{\tau}_{Bi}$ to $\tau^*_{Ni}, \dot{\tau}^*_{Ni}, \ddot{\tau}^*_{Ni}, \tau^*_{Bi}, \dot{\tau}^*_{Bi}, \ddot{\tau}^*_{Bi}$

6. Model Tests and Validation

6.1 Theoretical Background

The model testing technique is based on a non-dimensional formulation of the basic equations. In order to achieve model similarity, lengths are normalized by H/w, forces are normalized by H, and times are normalized by $\sqrt{mH}/\mathrm{w}$. Other physical dimensions are composed of these three basic dimensions and are normalized accordingly.

The static behaviour of the pipeline is completely defined by Eq. (2) and its boundary conditions. This is transformed into the following non-dimensional equations:

$$(EI)^*\frac{\partial^2\varphi}{\partial s^{*2}} - \sin\varphi + (s^*-V^*)\cos\varphi = 0$$

$$z^*(s^*=L^*) = \begin{cases} d^*-R^*(1-\cos\varphi(s^*=L^*)) & \text{if S method} \\ d^* & \text{if J-method} \end{cases}$$

$$\frac{\partial\varphi}{\partial s^*}(s^*=L^*) = \begin{cases} -1/R^* & \text{if S-method} \\ 0 & \text{if J-method} \end{cases}$$

$$x^*(s^*=0) = z^*(s^*=0) = \varphi(s^*=0) = \frac{\partial\varphi}{\partial s^*}(s^*=0) = 0$$

where the non-dimensional magnitudes are

non-dimensional curve length:	$s^* = \frac{\mathrm{w}s}{H}$
non-dimensional independent parameters:	$(EI)^* = \frac{EI\mathrm{w}^2}{H^3}$, $d^* = \frac{\mathrm{w}d}{H}$, $R^* = \frac{\mathrm{w}R}{H}$
the non-dimensional dependent parameters:	$V^* = \frac{V}{H}$, $L^* = \frac{\mathrm{w}L}{H}$
non-dimensional elastic line:	$x^* = \frac{\mathrm{w}x}{H}$, $z^* = \frac{\mathrm{w}z}{H}$

As the static behaviour of the pipeline depends only on $\frac{EI\mathrm{w}^2}{H^3}$, $\frac{\mathrm{w}d}{H}$ and $\frac{\mathrm{w}R}{H}$, for static model tests only these three non-dimensional parameters must have the same values in the model and in full-scale. The pipeline cross section must not be similar because the elastic state is completely defined by the shape of the pipe axis and by the effective tension force. If it is not similar, however, stresses may not be transformed directly to full-scale; instead the curvature and tension force are used for calculating the bending and normal stresses, respectively.

The dynamic behaviour of the pipeline is defined by Eqs. (9)-(11) and their boundary conditions. For simplicity, normalization is explained for the planar case, the direct hydrodynamic load p_N is neglected in comparison to the inhomogeneous boundary conditions due to the vessel's motion, the span laying on the soil is not considered, and the vessel's motion is assumed to be harmonic and unidirectional. Eqs. (9) and (11), simplified and transformed into a non-dimensional form, yield:

$$(EI)^*\frac{\partial^4 u^*}{\partial s^{*4}} - \frac{\partial}{\partial s^*}\left(F_s^*\frac{\partial u^*}{\partial s^*}\right) + \frac{\partial^2 u^*}{\partial t^{*2}} + c_d^*\left|\frac{\partial u^*}{\partial t^*}\right|\frac{\partial u^*}{\partial t^*} = \frac{\partial\varphi}{\partial s^*}F_{sdy}^*$$

$$F_{sdy}^* = \frac{(EA)^*}{L^*}\left[u_{sL}^* - \int_{(L^*)}\left(u^*\frac{\partial\varphi}{\partial s^*} - \frac{1}{2}\left(\frac{\partial u^*}{\partial s^*}\right)^2\right)ds^*\right];$$

boundary conditions: $u^*(s^*=L^*,t^*) = \hat{u}_{NL}^*\sin(\omega^* t^*)$; $\quad u_{sL}^*(t^*) = \hat{u}_{sL}^*\sin(\omega^* t^*)$

where the non-dimensional magnitudes, as far as they weren't explained yet together with the static problem, are

non-dimensional time: $$t^* = \frac{wt}{\sqrt{mH}}$$

non-dimensional bending deflections: $$u^* = \frac{wu_N}{H}$$

non-dimensional independent parameters: $$\omega^* = \frac{\omega\sqrt{mH}}{w},\ \hat{u}^*_{NL} = \frac{w\hat{u}_{NL}}{H},\ \hat{u}^*_{sL} = \frac{w\hat{u}_{sL}}{H},$$
$$(EA)^* = \frac{EA}{H},\ c^*_d = c_d \frac{\varrho}{2} D \frac{H}{wm}$$

As long as the pipeline behaves linearly, the amplitudes of the vessel's motions are not relevant, since the dynamic response is proportional to the motion amplitude. If there are nonlinearities, however, the non-dimensional amplitudes of the lateral and axial excitation, $\frac{w\hat{u}_{NL}}{H}$ and $\frac{w\hat{u}_{sL}}{H}$, should have the same values in model and full-scale. Restricting investigations to unidirectional motion of the lift-off point, the non-dimensional boundary pipe motion can be expressed by a single non-dimensional amplitude and the angle versus lateral direction.

To achieve model similarity of the drag force, the non-dimensional damping parameter $c_d \frac{\varrho}{2} D \frac{H}{wm}$ has to be maintained. This will be explained later in detail.

EA can be imagined as the tension force which would elongate a pipe span to the double of its original length. It is extremely high as compared to any existing force, e.g. H. Thus, the model pipeline has to comply with the merely qualitative similarity law $\frac{EA}{H} \gg 1$. Steel and similarly stiff metals satisfy this condition; a weighted rubber band, however, would not resemble a steel pipeline.

The above non-dimensional equations refer only to the free span. If the span laying on the ground is included, some additional non-dimensional numbers arise, describing the mechanical properties of the soil. As they are widely varying and have only moderate influence on the behaviour of the unsupported span, exact soil similarity has not been aimed at. It is sufficient to support the model pipeline by an elastic soil model long enough for damping to avoid reflections at the end.

It was decided to express model similarity by the three most important parameters:
- non-dimensional depth $\frac{wd}{H}$
- non-dimensional flexural rigidity $\frac{EIw^2}{H^3}$
- non-dimensional frequency $\frac{\omega\sqrt{mH}}{w}$

Of course, any combination of these parameters yields modified characteristic numbers. Thus, as an alternative, the similarity can also be expressed in terms of $\frac{wd}{H}$, $\frac{EI}{wd^3}$ and $\omega\sqrt{\frac{md}{w}}$ (for details see *Clauss and Kruppa 1974*).

As manufacturing hundreds of model pipelines is time-consuming and expensive, the aim was to simulate a wide variety of full-scale problems with one single model pipeline. Thus, the parameters were split into two categories: i) parameters particular to the model pipeline, which cannot be varied and ii) parameters particular to each individual model test which are varied to establish model similarity.

The following quantities of the model pipeline had to be be selected once for ever (model quantities marked by *):

$(EI)^*$=flexural rigidity
w^* =submerged weight per length
m^* =effective mass per length (incl. hydrodynamic mass)
D^* =external diameter

Three parameters are easily adapted to full-scale similarity:

H^*=static horizontal force
d^* =vertical depth from the bottom to the upper end of the unsupported span
ω^* =circular frequency of excitation

To simulate a specific full-scale problem with the available model pipeline, the three similarity laws are considered an equation system, where H^*, d^* and ω^* are the unknowns:

$$\text{Horizontal force:} \quad \frac{EI\mathrm{w}^2}{H^3} = \frac{(EI)^*\mathrm{w}^{*2}}{H^{*3}} \quad \Rightarrow \quad H^* = H\left(\frac{(EI)^*\mathrm{w}^{*2}}{EI\mathrm{w}^2}\right)^{1/3} \tag{37}$$

$$\text{Depth:} \quad \frac{\mathrm{w}d}{H} = \frac{\mathrm{w}^*d^*}{H^*} \quad \Rightarrow \quad d^* = d\left(\frac{(EI)^*\mathrm{w}}{EI\mathrm{w}^*}\right)^{1/3} \tag{38}$$

$$\text{circular frequency:} \quad \frac{\omega\sqrt{mH}}{\mathrm{w}} = \frac{\omega^*\sqrt{m^*H^*}}{\mathrm{w}^*} \quad \Rightarrow \quad \omega^* = \omega\left(\frac{m}{m^*}\right)^{1/2}\left(\frac{EI}{(EI)^*}\right)^{1/6}\left(\frac{\mathrm{w}^*}{\mathrm{w}}\right)^{2/3} \tag{39}$$

From these equations, the scales of the three basic dimensions, i.e. length, force and time, can be expressed by magnitudes known from the full-scale problem and the available model cross section, i.e. eliminating the initially unknown parameters H^*, d^* and ω^*:

$$\text{length scale} = \lambda_l = \frac{d}{d^*} = \left(\frac{EI\mathrm{w}^*}{(EI)^*\mathrm{w}}\right)^{1/3} \tag{40}$$

$$\text{force scale} = \lambda_f = \frac{H}{H^*} = \left(\frac{EI\mathrm{w}^2}{(EI)^*\mathrm{w}^{*2}}\right)^{1/3} \tag{41}$$

$$\text{time scale} = \lambda_t = \frac{T}{T^*} = \frac{\omega^*}{\omega} = \left(\frac{m}{m^*}\right)^{1/2}\left(\frac{EI}{(EI)^*}\right)^{1/6}\left(\frac{\mathrm{w}^*}{\mathrm{w}}\right)^{2/3} = \left(\frac{m}{m^*}\frac{\lambda_l^2}{\lambda_f}\right)^{1/2} \tag{42}$$

This ensures model similarity of all relevant effects except drag forces, the similarity of which is checked now. As mentioned previously, the related characteristic number still to be discussed is

$$c_d\frac{\varrho}{2}D\frac{H}{\mathrm{w}m} = c_d^*\frac{\varrho^*}{2}D^*\frac{H^*}{\mathrm{w}^*m^*} \quad .$$

Introducing $\frac{H}{\mathrm{w}d} = \frac{H^*}{\mathrm{w}^*d^*}$, $\frac{d}{d^*} = \lambda_l$ and $\frac{m}{m^*}$ from Eq.(42) and assuming that $\varrho \approx \varrho^*$, this yields the model similarity law of the hydrodynamic drag:

$$\frac{D}{D^*} = \frac{c_d^*}{c_d}\frac{\varrho^*}{\varrho}\frac{H^*}{H}\frac{\mathrm{w}}{\mathrm{w}^*}\frac{m}{m^*} = \frac{c_d^*}{c_d}\frac{\mathrm{w}d/H}{\mathrm{w}^*d^*/H^*}\frac{d^*}{d}\frac{m\lambda_l^2}{m^*\lambda_f}\frac{\lambda_f}{\lambda_l^2} = \frac{c_d^*}{c_d}\frac{\lambda_t^2\lambda_f}{\lambda_l^3} \tag{43}$$

As D is not contained in any other parameter, the ratio D/D^*, which is not the length scale, may be selected independently to satisfy the drag similarity law Eq. (43). It would be mathematically correct, but practically not feasible, to treat the external diameter D^* of the model cross section as a fourth variable parameter to be adjusted previously to each individual model test (like H^*, d^* and ω^*). Instead, the model cross section was designed with a diameter to satisfy the drag similarity law, Eq. (43), as precise as possible for all the range of full-scale problems to be simulated.

The drag coefficient is a function of the Reynolds number Re and the Keulegan-Carpenter number KC. In our case the full-scale Reynolds number is about 100 times that of the model, whereas the KC-numbers are comparable. For details see *Clauss et al. (1988)*.

6.2 The Model Pipeline

The model pipeline (Fig. 2), designed for bending in one plain, consists of a rectangular stainless steel strip (20 mm x 2 mm) surrounded by elements of perspex pipe (30mm external diameter, wall thickness 3 mm). The core of the model pipeline, i.e. the massive rectangular steel strip, determines the flexural rigidity and ensures that the axial rigidity is extremely high as desired. In order to avoid any influence on the flexural rigidity, the perspex pipe is divided into segments of 20 cm length, each of them attached to the flat steel profile with screws at both ends, providing sufficient space for bending between the segments. For stress measurements, the steel profile is equipped with strain gauges in distances of about 60 cm. The submerged weight per unit length results mainly from the steel strip, with a small addition from the submerged perspex pipe. Both the steel strip and the perspex pipe contribute to the effective mass per unit length which also includes the water trapped inside the pipe and the 'outer' hydrodynamic added mass.

Model pipeline specifications:

submerged weight per unit length	w*	$=3.5646\ N/m$
effective mass per unit length	m^*	$=1.7771\ kg/m$
flexural rigidity	$(EI)^*$	$=2.7467\ Nm^2$
axial rigidity	$(EA)^*$	$=8.24 \cdot 10^6 N$
external diameter	D^*	$=0.03\ m$

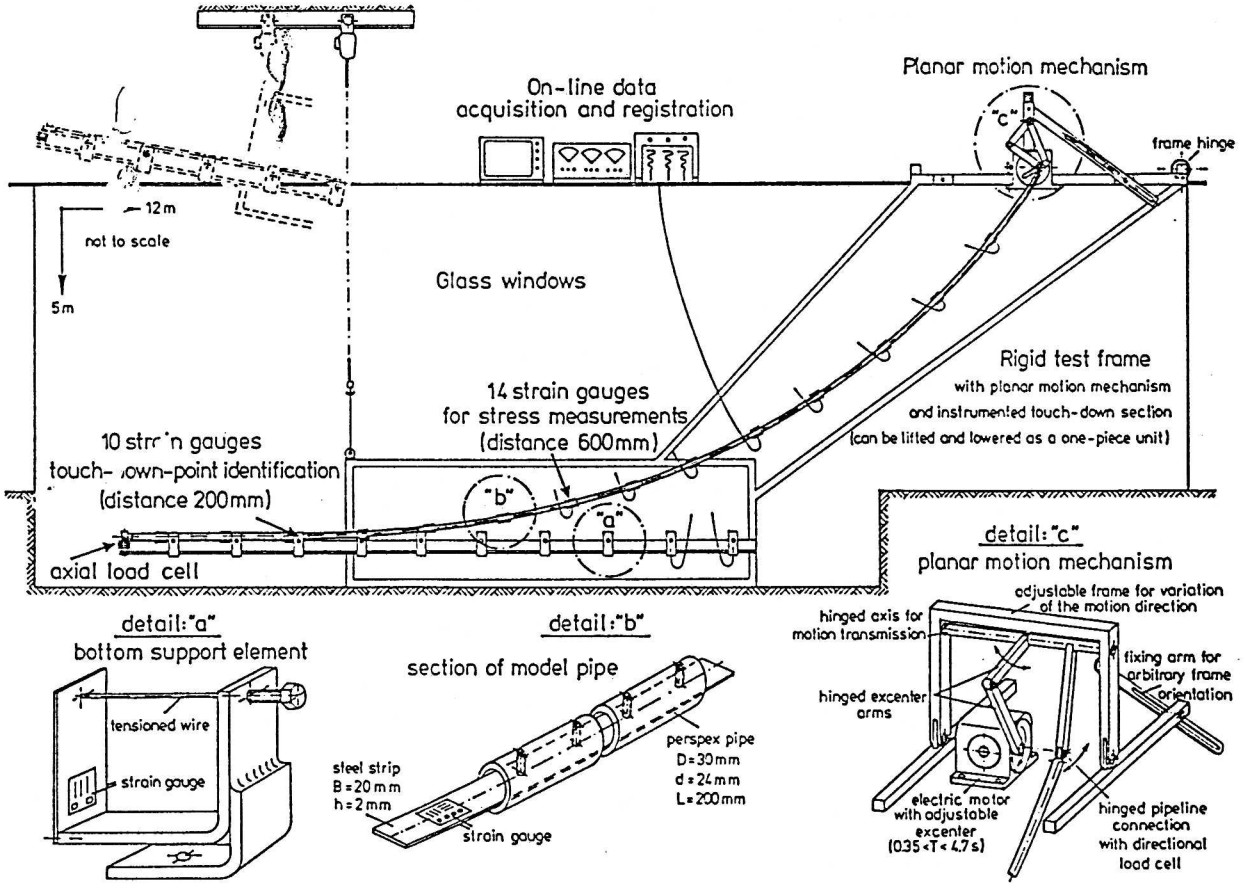

Fig.2: Model Testing Technique

6.3 The Test Facility

The experiments were carried out in the deep water tank of our institute having 12 m length, 1.3 m width and about 5 m depth. The planar motion mechanism and the bottom supports of the pipeline beyond the touch-down point were attached to a large steel frame which is movable around a bearing at the tank top (Fig. 2). Thus, the lower end of the pipeline can be lifted easily so that all equipment is accessible above the water surface, with the pipeline suspended between two points at the same level.

To simulate the laying vessel's motions in the seaway, the upper end of the pipeline is hinged to a planar motion mechanism providing unidirectional harmonic oscillations whose motion direction, amplitude and frequency can be varied arbitrarily.

At the opposite end, the pipeline lays on a model 'seabed', which can be fixed horizontally at different depths d^* below the upper end. To simulate soil elasticity, the soil model consists of a series of U-shaped steel elements bridged with a tensioned steel wire. The pipe, after touch-down, is supported by these steel wires, their tension being adjusted with screws to represent a defined subgrade modulus. Such bottom supports are positioned at distances of 20 cm. The first five of them are equipped with strain gauges to detect the touch-down point. At the end of this soil model the pipe is attached to a load cell. Its position can be shifted horizontally to adjust the static horizontal force.

The static shape of the pipeline is registered with a sensor which can be moved to different horizontal coordinates and lowered until contact with the pipeline is detected, thus defining the vertical coordinate.

6.4 The Model Tests

The purpose of the model tests was not to simulate full-scale problems, but to validate the theory. Nevertheless, model similarity is necessary to ensure that the validation takes place within a realistic range of parameters. The results of model scale calculations and model tests are compared.

From all available publications of planned or executed pipelaying projects, a file was made which allows to extract the parameters w, H, d, EI, R and m. Since H and R are missing in most publications, R was selected to correspond to $300\,N/mm^2$ static bending stress on the stinger, and the required horizontal force H is calculated for the S-method to limit the maximum static bending stresses to $300N/mm^2$ and the required stinger length to $150m$.

Applying the previously developed expressions for length, force and time scale, a corresponding file was generated listing the model horizontal force H^*, the lowest excitation period corresponding to a full-scale wave period of $4s$ and the height and length of the model pipe arrangement to check the feasibility of a model test.

Two typical examples are:

location	Frigg-Karmøy *Lund (1976)*	Strait of Messina *Anonymus (1979)*
ext. diameter of steel pipe	406.0 mm	508.0 mm
steel wall thickness	15.9 mm	23.8 mm
concrete coating thickness	63.5 mm	0 mm
submerged weight per length w	1215.7 N/m	843.66 N/m
effective mass per length m	582 kg/m	501.50 kg/m
flexural rigidity EI	76.7 $MN \cdot m^2$	219.09 $MN \cdot m^2$
laying depth d	150 m	237 m
horizontal force H	333 kN	279 kN
length scale λ_l	43.477	69.597
force scale λ_f	14827	16471
time scale λ_t	6.458	9.110

Two types of results are obtained from the model tests:

- long time photographs of small light-emitting diodes attached to the pipeline to register trajectories
- time series (using our proven model testing software developed by Weede et al.) from:
  - ▷ strain gauges located along the pipeline,
  - ▷ the load cell at the bottom
  - ▷ the directional load cell at the top, the signals of which were geometrically transformed to the force component in the oscillating direction axial to the pipe

The trajectory photographs are compared with theoretical results by linking the calculation subroutines to a program which draws trajectories in exactly the same scale. Results referring to the Messina pipeline are presented in Figs. 3 and 4.

The measured time series of each model test were compared to a theoretical simulation. Fig. 5 shows theoretical (left) and model test results (right) for the Frigg-Karmøy pipeline. The figures represent the pipeline's behaviour at four different frequencies, starting with an extremly slow motion in the upper diagrams. The dynamic bending stresses were interpolated between the strain gauges with the parabolic blending method. The shape of the stress curves at the lowest frequency (upper diagrams) has one node in the free pipe span suggesting the second mode shape. However, this variation of the stress along the pipeline results from the varying positions of the hinged upper end of the pipeline and the associated steady-state pipe geometries. At higher frequencies, the number of nodes increases, and the dynamic response is influenced by nonlinear interaction between bending and tension and by hydrodynamic damping. The calculated stresses compare well with the measured ones. The upper and lower stress diagrams are accompanied by time series of the dynamic tension force. As theory compares well with measured data for the slowest and fastest motion, the dynamic tension forces for the other frequencies are not shown. These time series clearly show the nonlinear behaviour. For confirming Kirchhoff's hypothesis (*Kauderer 1958)* that the dynamic tension does not vary along the pipeline, it was measured at both ends of the pipeline. The lowest diagram on the right side shows that both load cell signals, indeed, are equal.

7. Full-Scale Calculations

Example calculations for the Messina Pipeline have been performed to illustrate the influence of the following parameters: wave period T, the vessel's motion direction and amplitude at the lift-off point, the static horizontal force H and the depth d. Figs. 6 ff. illustrate the dynamic bending deflection and the corresponding stresses for different values of these parameters. Note that the stresses are presented at the upper and lower fiber of the pipeline superimposing the static stress and the envelope of the dynamic effects.

The figures show also the differences between the two modes of tensioner control:

- Blocked tensioner: The vessel fully imposes its motions to the upper end of the free pipe span in its tangent direction. This yields large oscillations of tension force.
- Compensating tensioner: The two caterpillar tracks which grip the pipe provide exactly the relative axial motion required to keep the tension force on a constant value. This motion, inside the welding station as well as at the lift-off point, is the difference between the bending-induced axial pipe deflection and the vessel motion tangent to the pipe.

It is evident that any pipe laying procedure has to cope with either high variations of the tension force or relative axial motions between pipe and vessel. Tension force peaks beyond the tensioner capacity may cause the tensioner either to squeeze the pipe or to damage the concrete coating, and large tension force variations mutually cause large bending oscillations. Relative axial motions, on the other hand, are disadvantageous for manufacturing. In general, small motions of the pipelaying vessel are advantageous for operations both with blocked and compensating tensioner, which explains the preference for semisubmersible laying vessels.

8. Conclusions

The paper describes and validates a large deflection dynamic analysis method for submerged circular beams, stiffened by a longitudinally variable tension force and exposed to boundary-value induced bending vibrations interacting with a dynamic tension force. To a frequency domain finite element solution a modally decomposed contribution from the nonlinear effects is superimposed in the time domain. The method is applied to the suspended free span of an offshore pipeline being installed from a vessel oscillating in the seaway. The boundary conditions particular to offshore pipelaying include soil mechanics at the bottom and a sophisticated control of the tensioning machine at the top.

Dynamic effects pose severe problems for pipelaying in rough sea conditions, especially if the laying vessel moves substantially in short waves. Blocking of the tensioner results in extremly high axial dynamic forces which may cause the tensioner to damage the pipe when trying to retain it. Operating the tensioner with constant tension force is associated with axial motions between laying vessel and pipeline with which the manufacturing procedure has to cope. Example calculations prove that dynamic effects should be taken into account at any laying operation. The calculation method for these effects is versatile, allowing adaptations to any specific laying problem.

References

BLIEK,A. and TRIANTAFILLOU,M.S. (1985), Nonlinear cable dynamics, Behaviour of Offshore Structures, Elsevier Science Publishers B.V., Amsterdam

BORGMAN,L.E. (1969), Ocean wave simulation for engineering design, Journal of the Waterways and Harbors Division, Proc. of the ASCE 95 / WW4

BRUSCHI,R., MONTESI,M., RAGAGLIA,R. and TURA,F. (1987), A new boundary element for free span analysis, Offshore and Arctic Pipelines

BURNETT, D.S. (1987), Finite element analysis, Addison-Wesley Publishing Company, Reading

CLAUSS,G.F., LEHMANN,E. and ÖSTERGAARD,C. (1988), Meerestechnische Konstruktionen, Springer-Verlag, Berlin

CLAUSS,G., KRUPPA,C., WOLF,E. and STAMM,K. (1977), Parameterstudie über das Verlegen von Pipelines in großen Meerestiefen, Meerestechnik 8 Nr.3 Juni

CLAUSS,G. and KRUPPA,C. (1974), Model testing techniques in offshore pipelining, OTC 1973 Houston

CLAUSS,G.F. and WEEDE,H.E.W. (1990), Dynamics of pipelines during laying operations, Offshore Engineering, Proc. of the 7th Int.Symp.on Offsh.Eng. held at COPPE, Fed.Univ. of R.J., Brazil, Aug.1989, Pentech Press, London

GARDNER,T.N. and KOTCH,M.A. (1976), Dynamic analysis of risers and raissons by the element method, OTC 2651, Houston

HAPEL,K. and KÖHL,M. (1980), Erzwungene Transversalschwingungen langer Drilling-Riser - der Dämpfungsparameter der linearisierten Widerstandskraft, Der Stahlbau 11

HOBBS, R.E. (1986), Influence of structural boundary conditions on Pipeline Free Span Dynamics, Proc. of the 5th OMAE Symposium, Tokyo

KAUDERER,H. (1958), Nichtlineare Mechanik, Springer-Verlag, Berlin/Göttingen/Heidelberg

KIRK,C.L. and ETOK,E.U. (1979), Wave induced random oscillations of pipelines during laying, Applied Ocean Research, Vol.1, No.1

KROLIKOWSKI,L.P. and GAY,T.A. (1980), An improved linearization technique for frequency domain riser analysis, OTC 3777, Houston

LANGNER,C.G. and AYERS,R.R. (1985), The feasibility of laying pipelines in deep waters, OMAE 85, Houston

LUND,S. (1976), Geplante Pipeline durch den Norwegischen Graben, Meerestechnik mt 7 Nr.5, Oktober

MALAHY,R.C. (1986), A nonlinear finite element method for the analysis of offshore pipelines, risers and cable structures, Proc. of the 5th OMAE Symposium, Tokyo

OLIVER,J. and OÑATE,E. (1985), A finite element formulation for the analysis of marine pipelines during laying operations, Journal of Pipelines, 5, pp.15-35

PEDERSEN,P.T. and YAN,J. (1986), 3-D static analysis of pipelines during laying, OTC 5297, Houston

ANONYMUS (1979), The gas pipeline from Algeria to Italy, Pipes & Pipelines International, Dec.

VLAHOPOULOS,N. and BERNITSAS,M. (1990), Three-dimensional nonlinear analysis of pipelaying, Applied Ocean Research, Vol.12, No.3

WEEDE,H. (1990), Dynamik offshoretechnischer Linientragwerke am Beispiel der Pipelineverlegung, Dissertation, TU Berlin

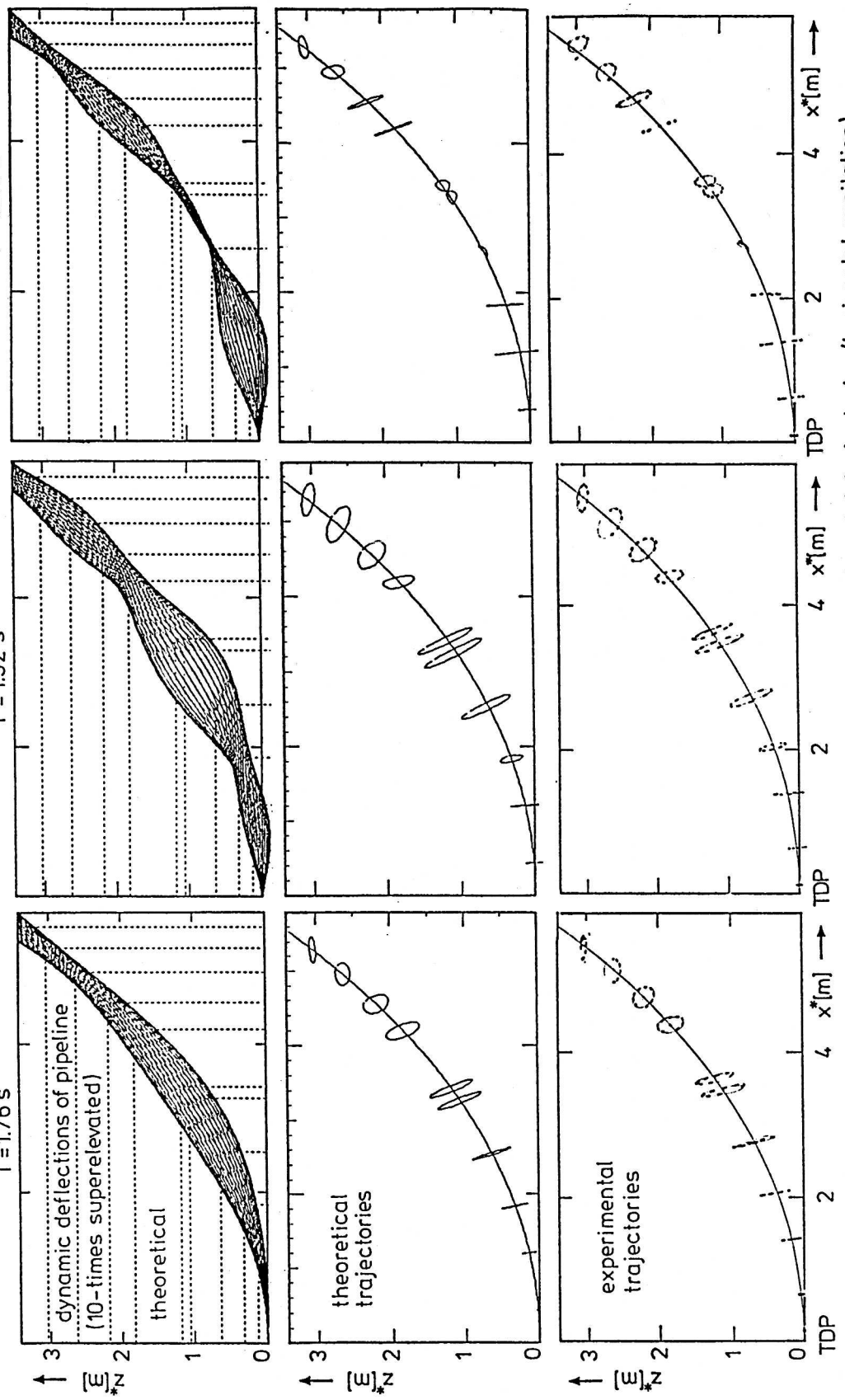

Fig. 3 Pipeline dynamics - comparison of theoretical and experimental trajectories (horizontal excitation)

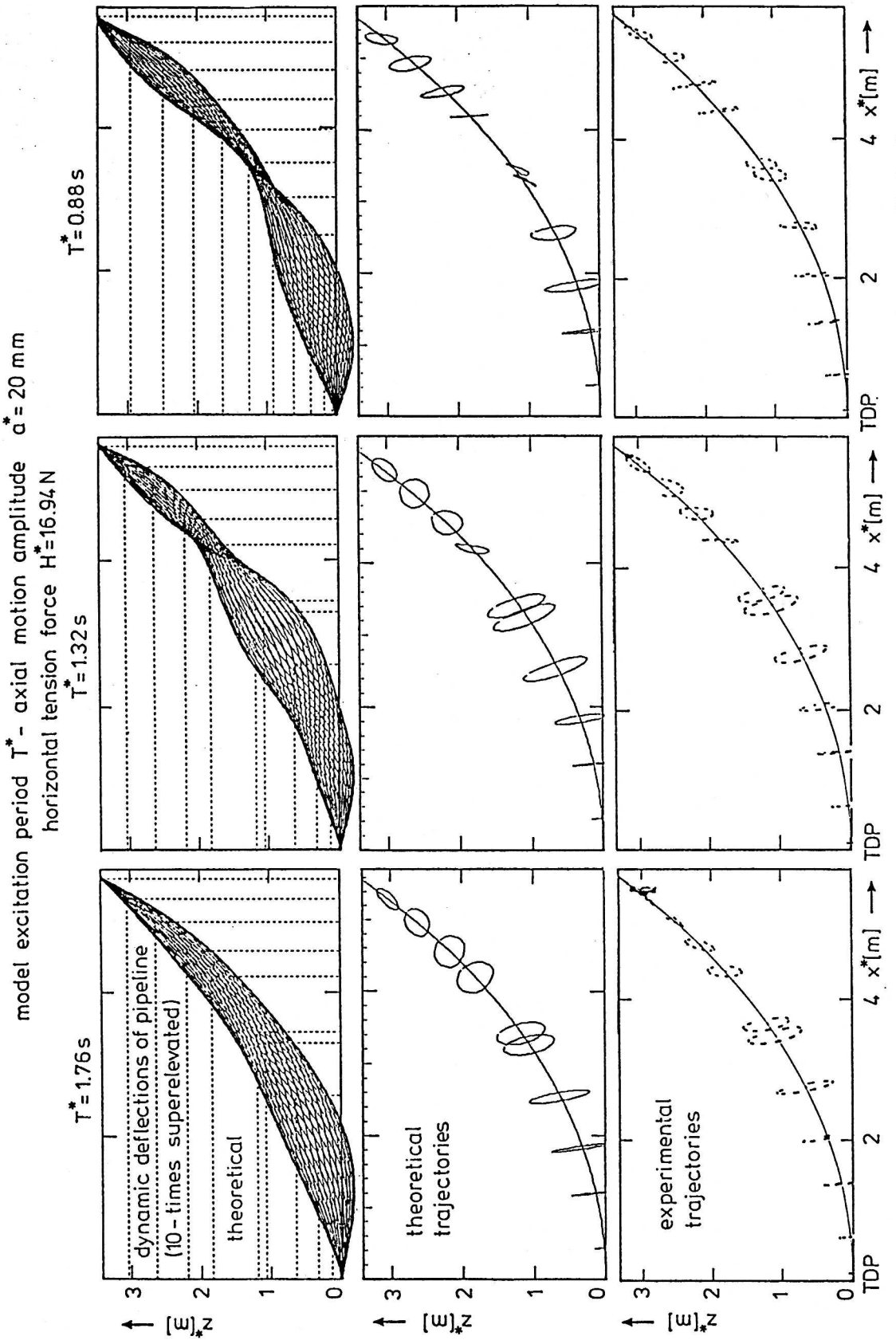

Fig.4 Pipeline dynamics - comparison of theoretical and experimental trajectories (axial excitation)

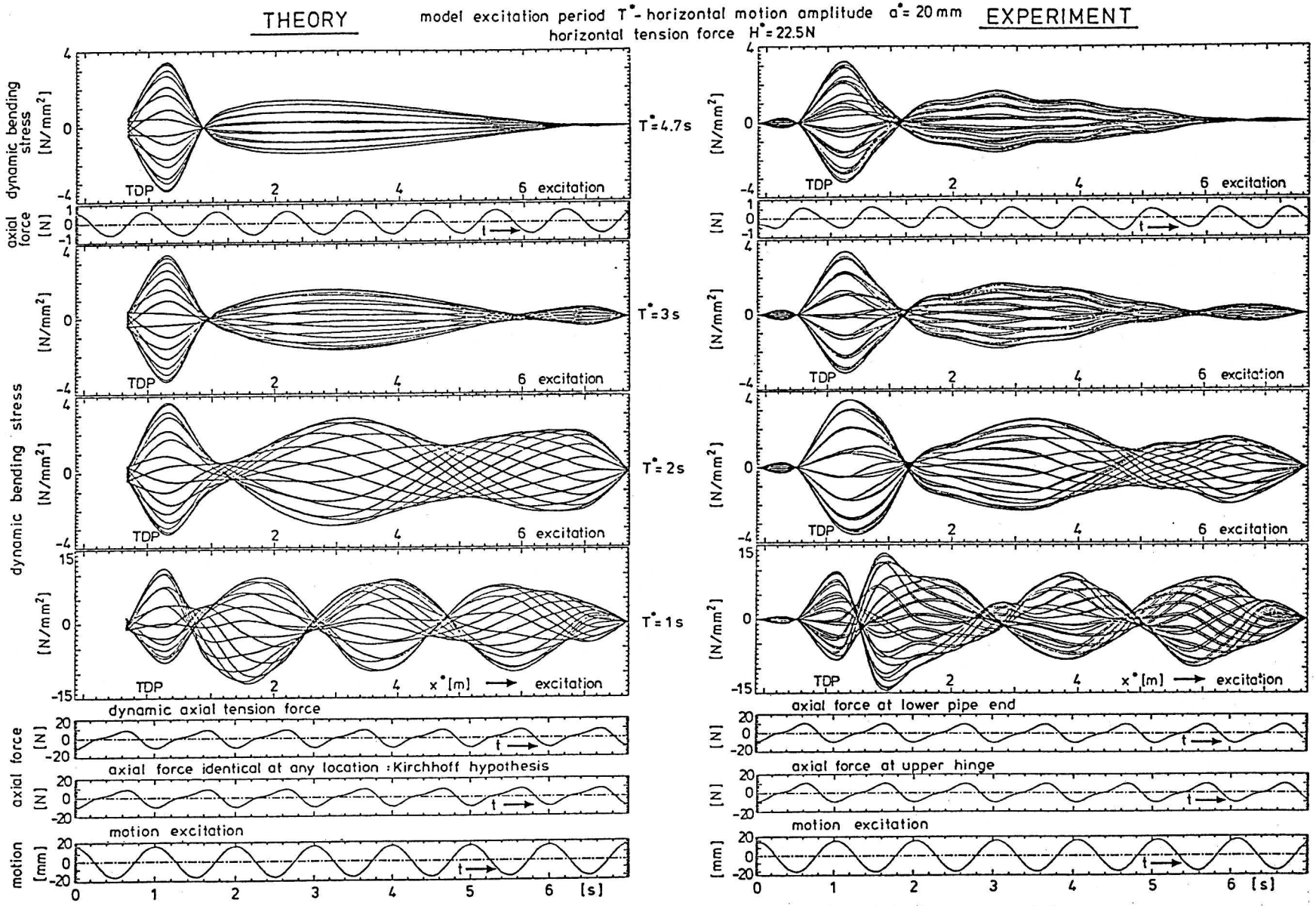

Fig. 5 Pipeline dynamics - comparison of theoretical and experimental stresses and forces

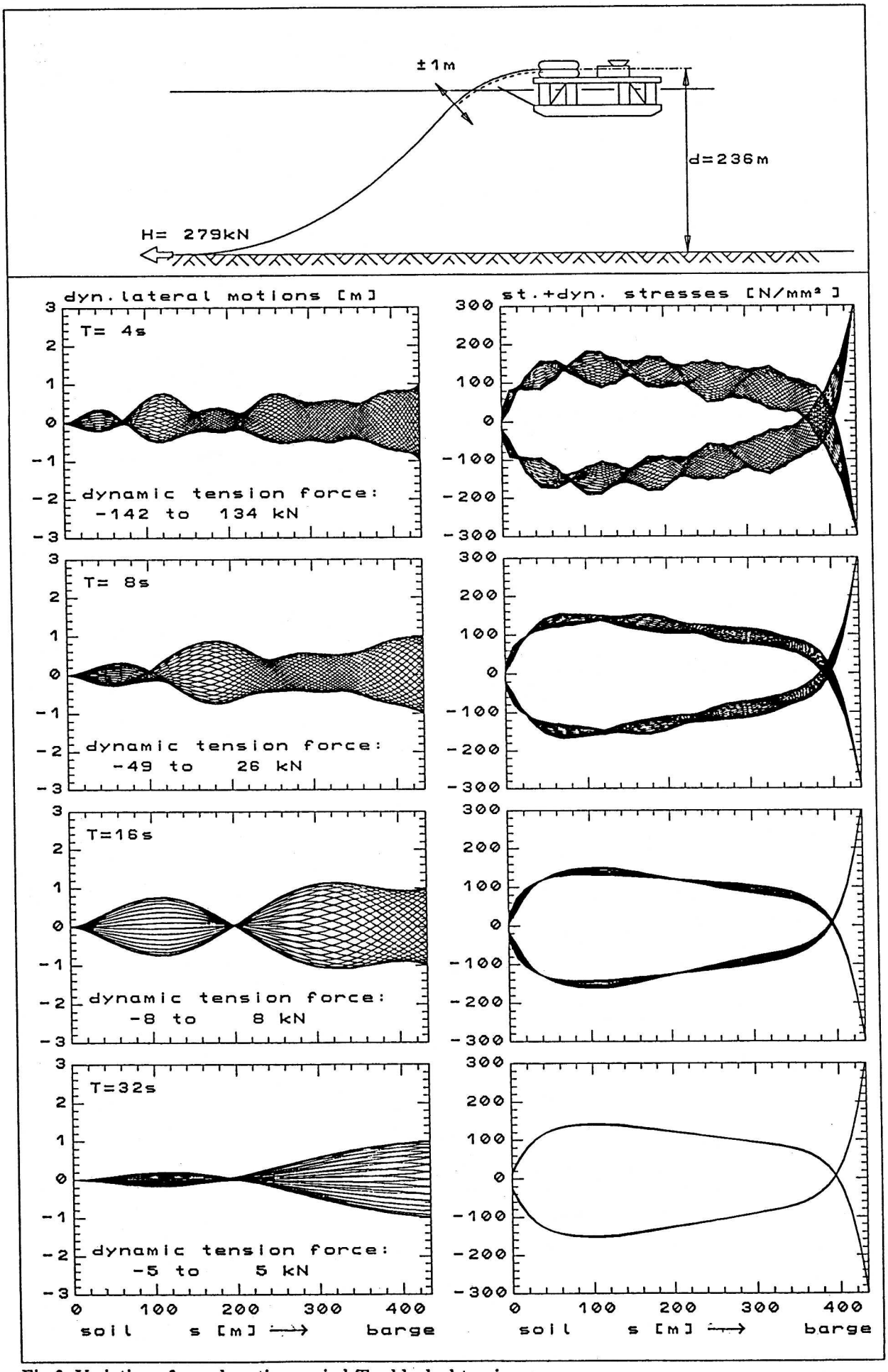

Fig.6: Variation of vessel motion period T – blocked tensioner

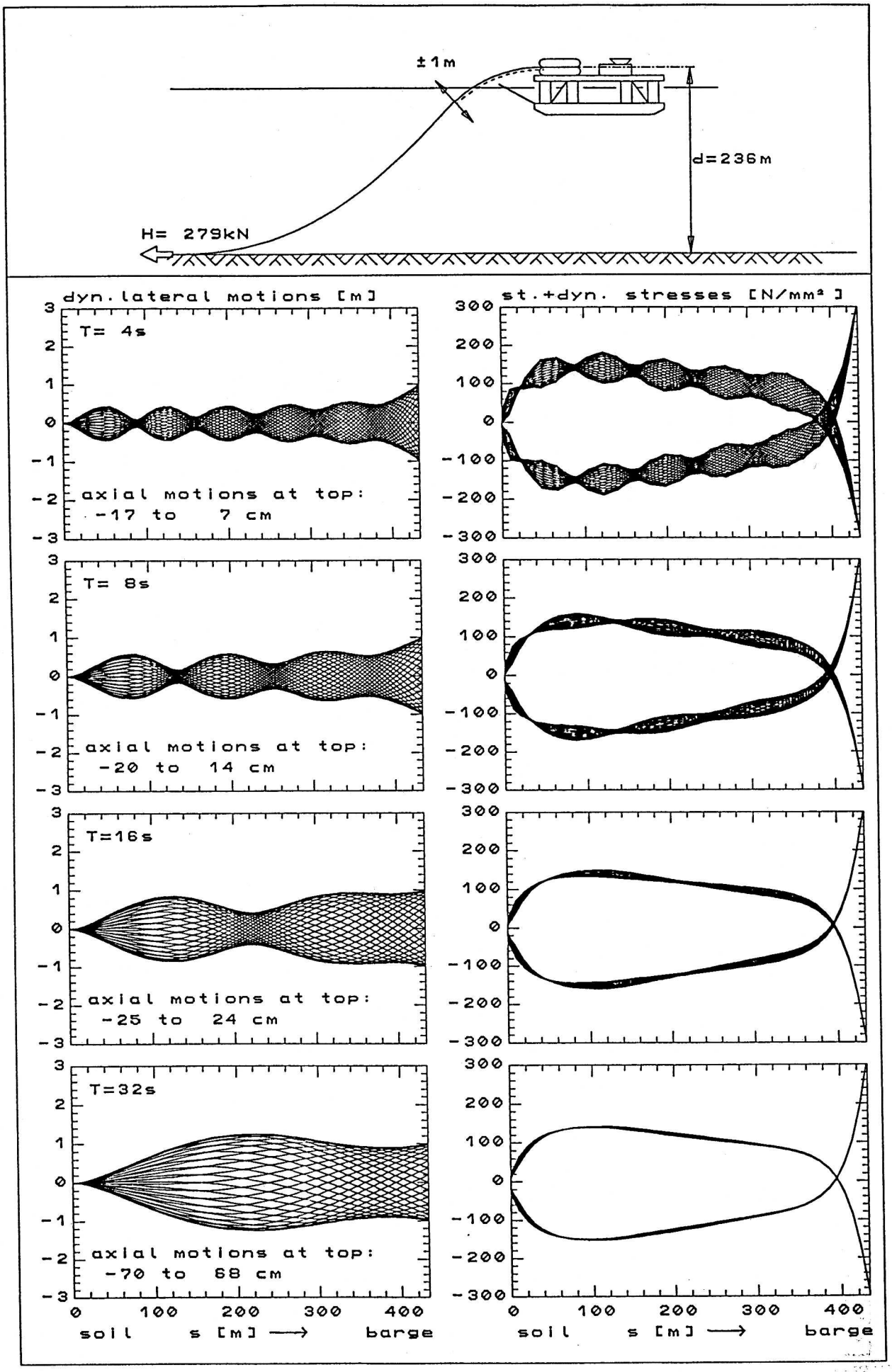

Fig.7: Variation of vessel motion period T – compensating tensioner

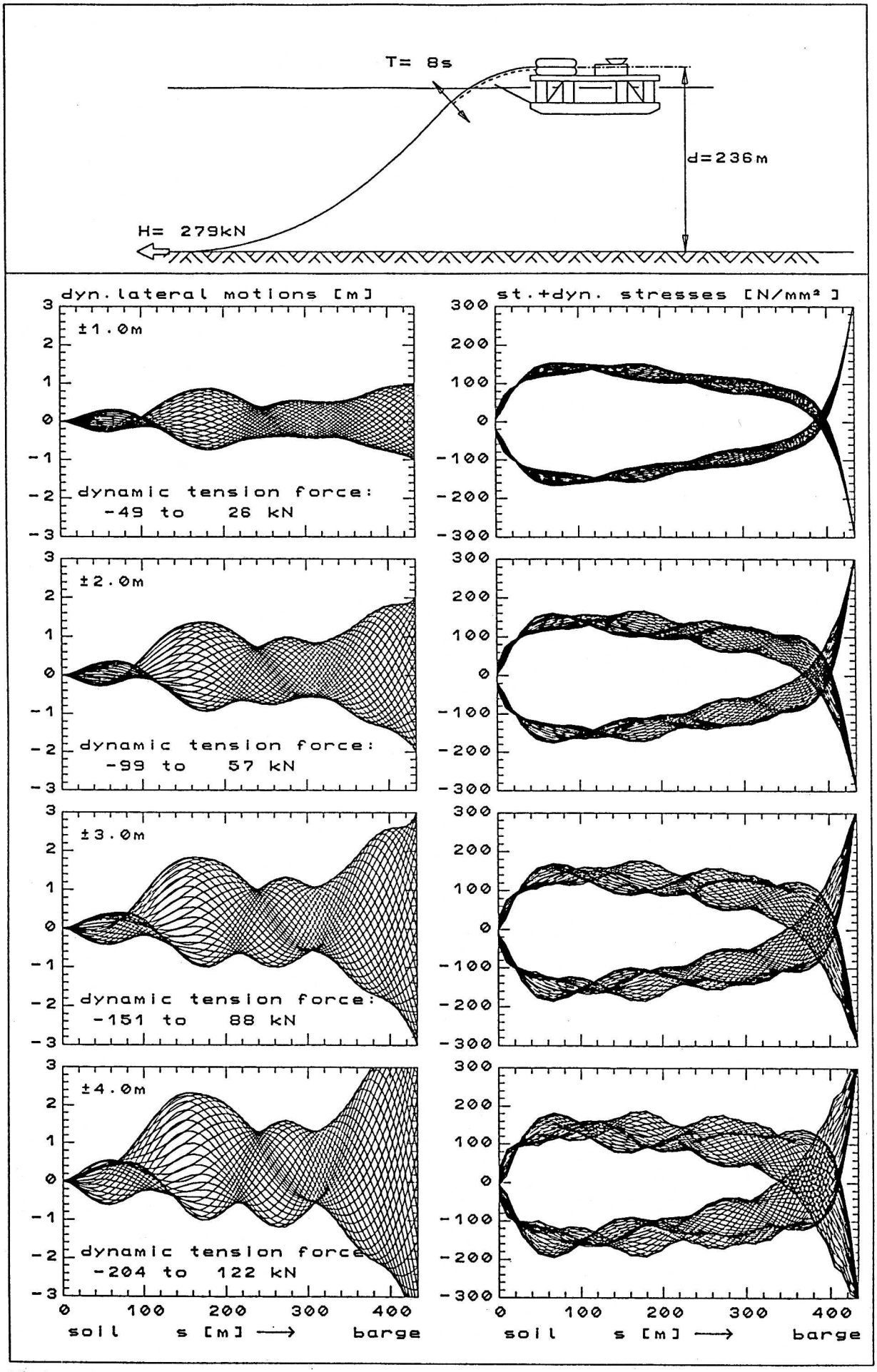

Fig.8: Variation of vessel motion amplitude – blocked tensioner

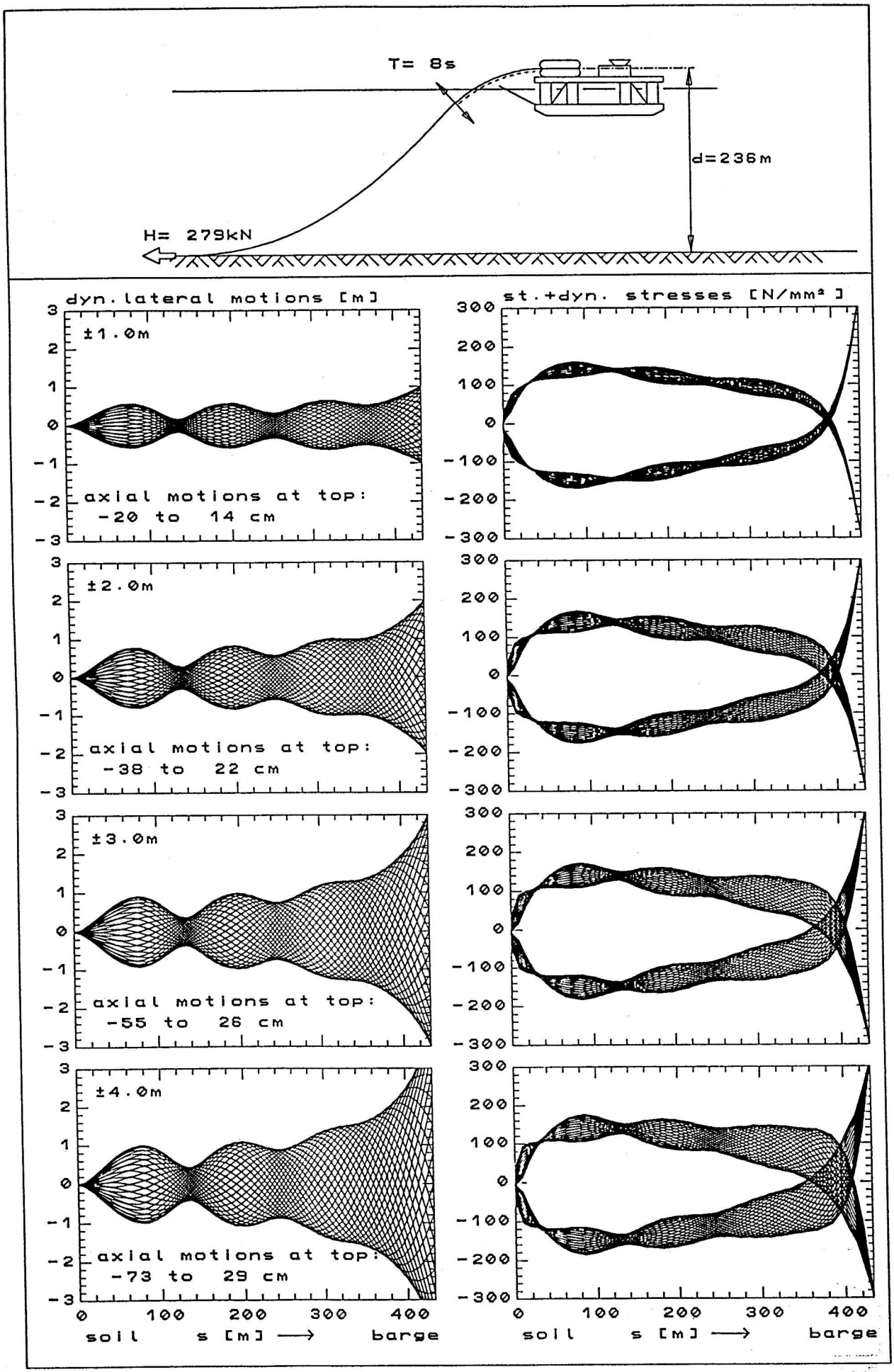

Fig.9: Variation of vessel motion amplitude – compensating tensioner

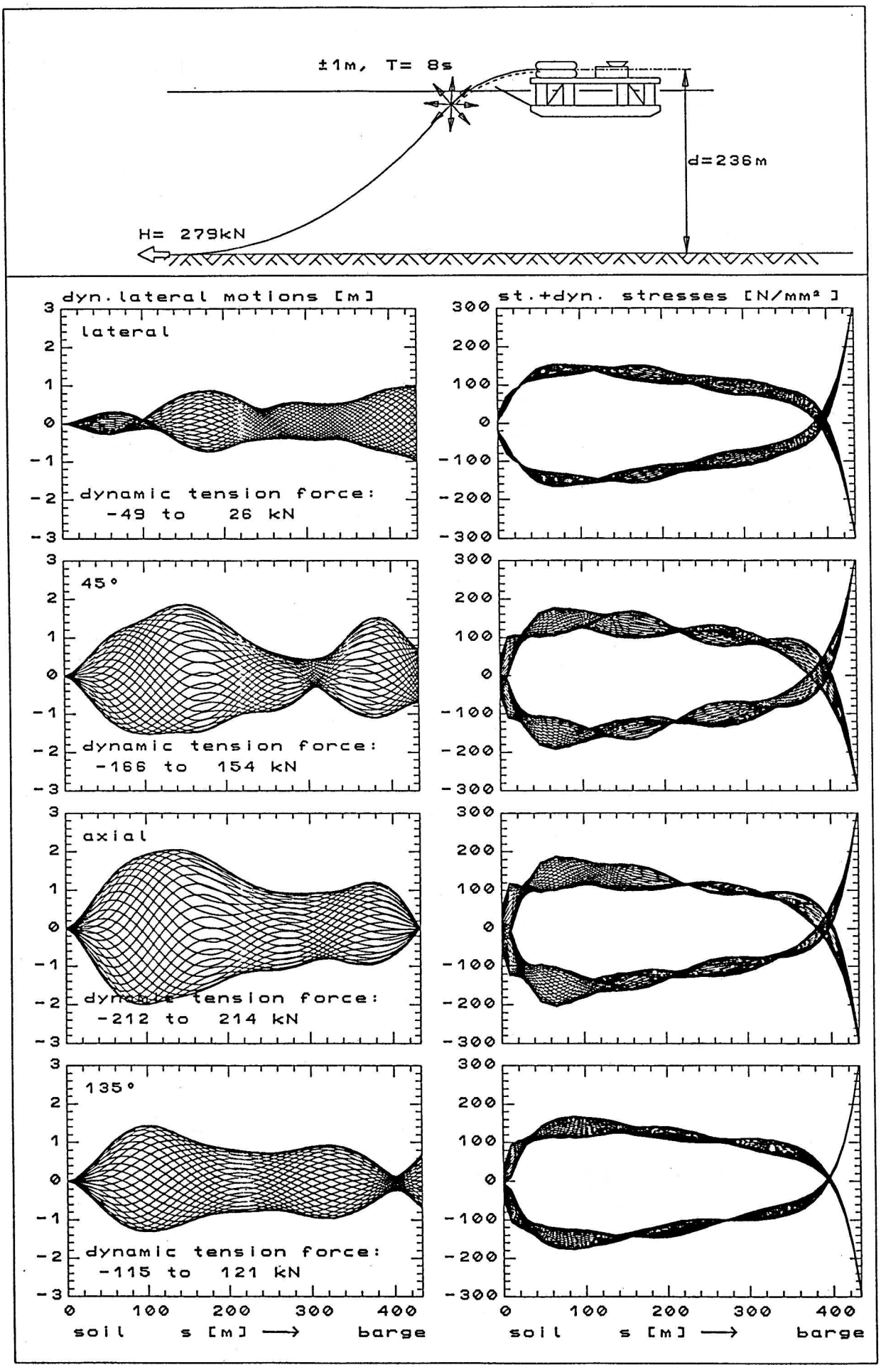

Fig.10: Variation of vessel motion direction – blocked tensioner

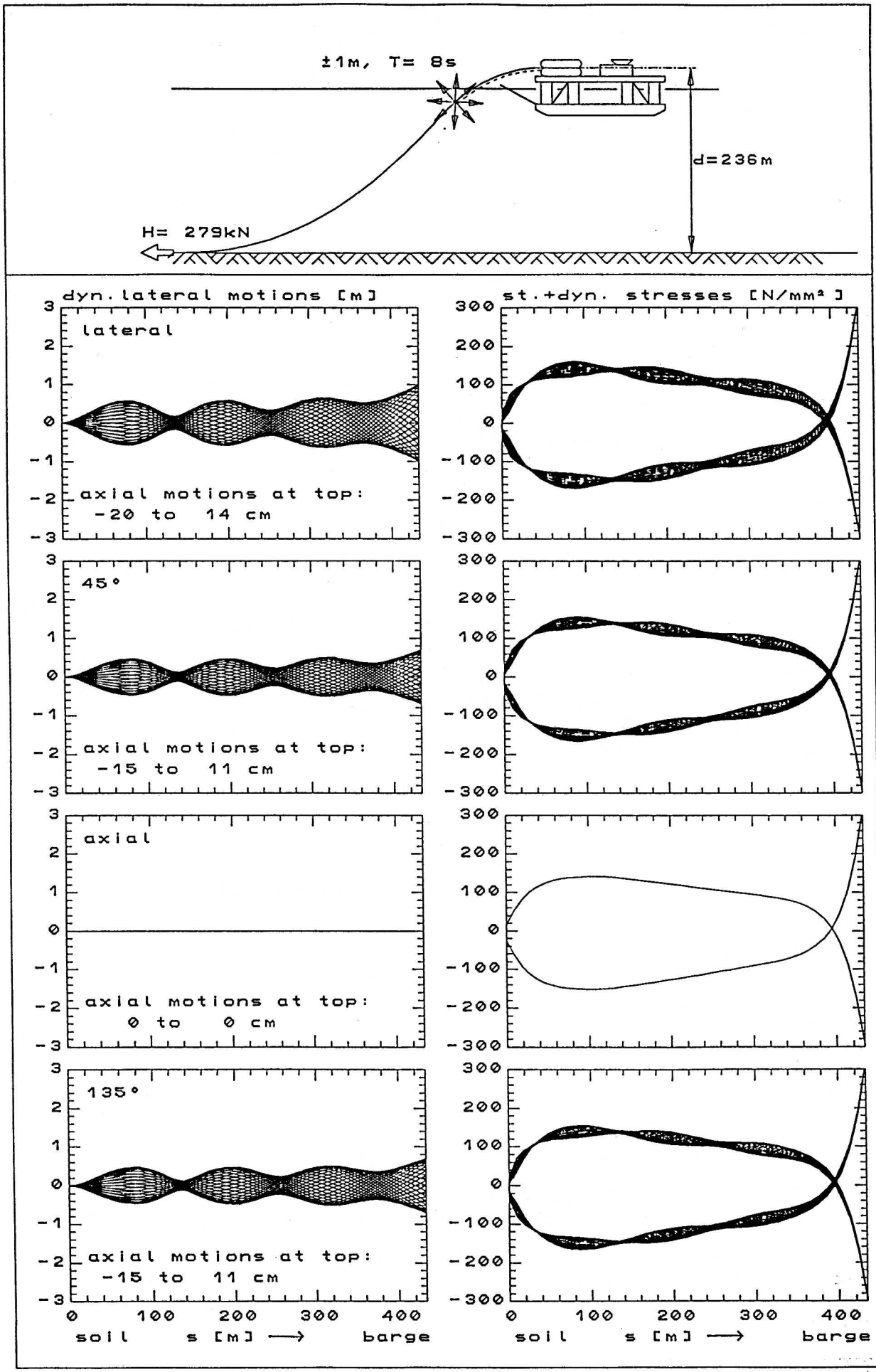

Fig.11: Variation of vessel motion direction – compensating tensioner

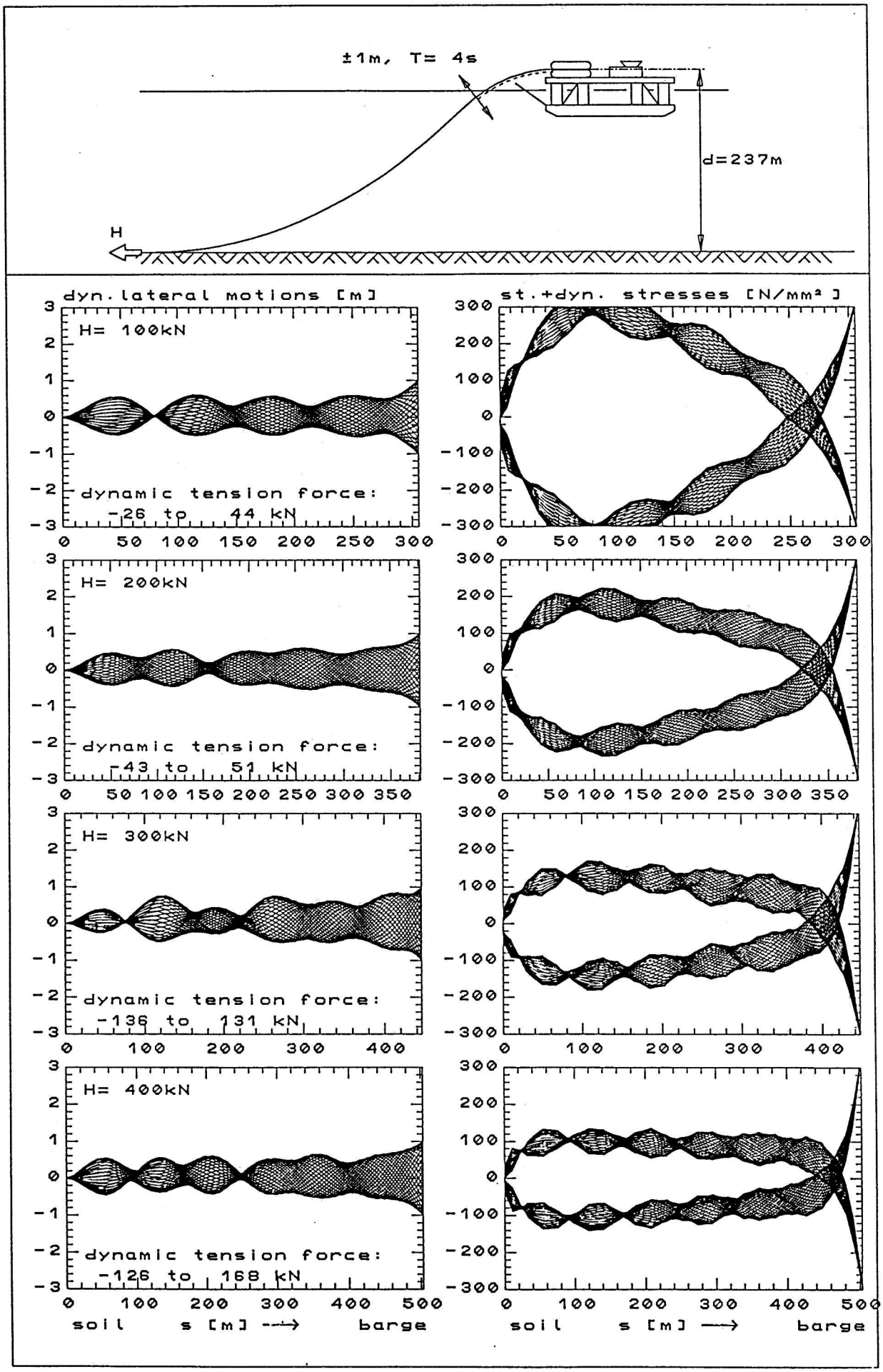

Fig.12: Variation of static horizontal force H – blocked tensioner

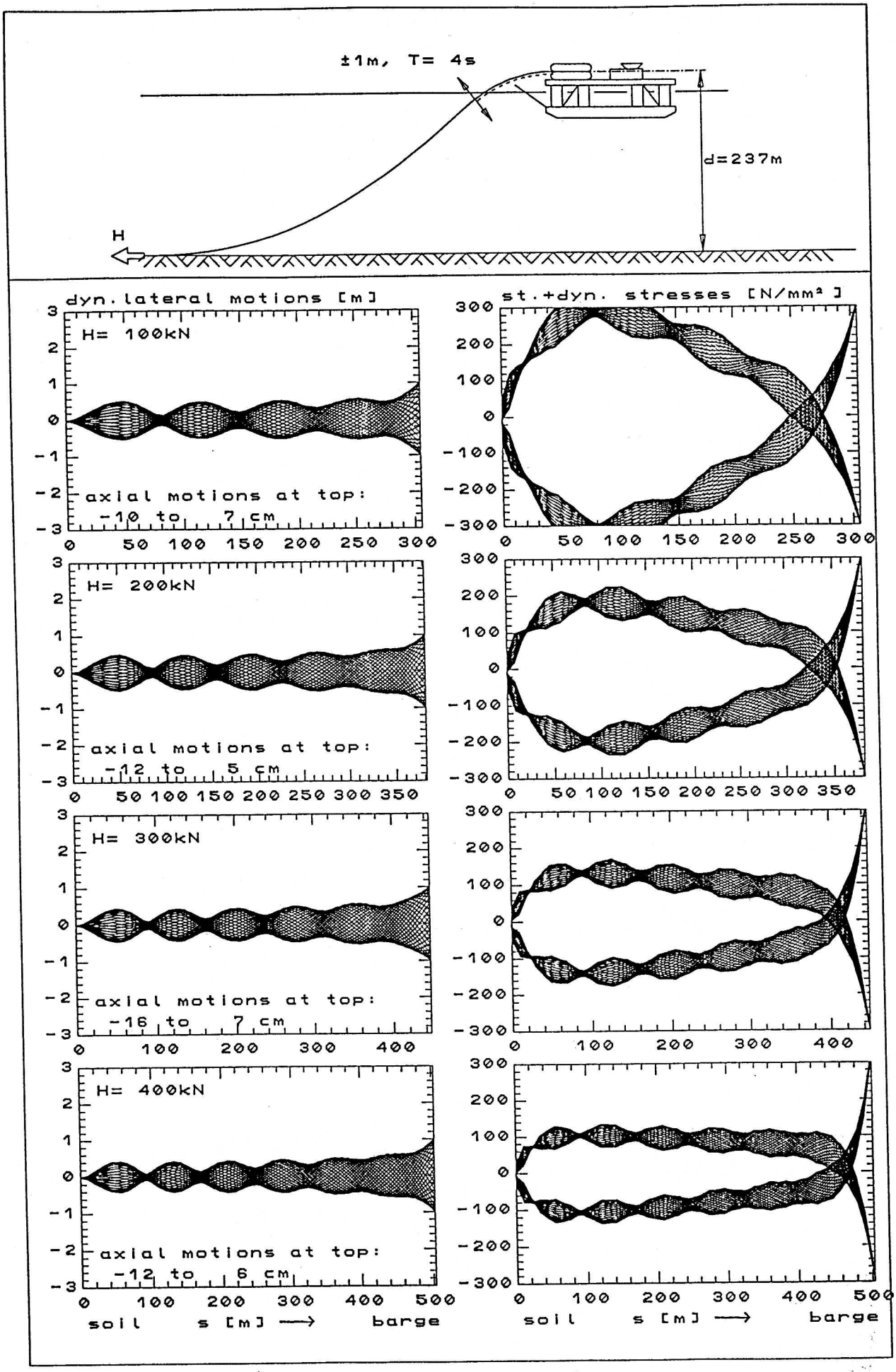

Fig.13: Variation of static horizontal force H – compensating tensioner

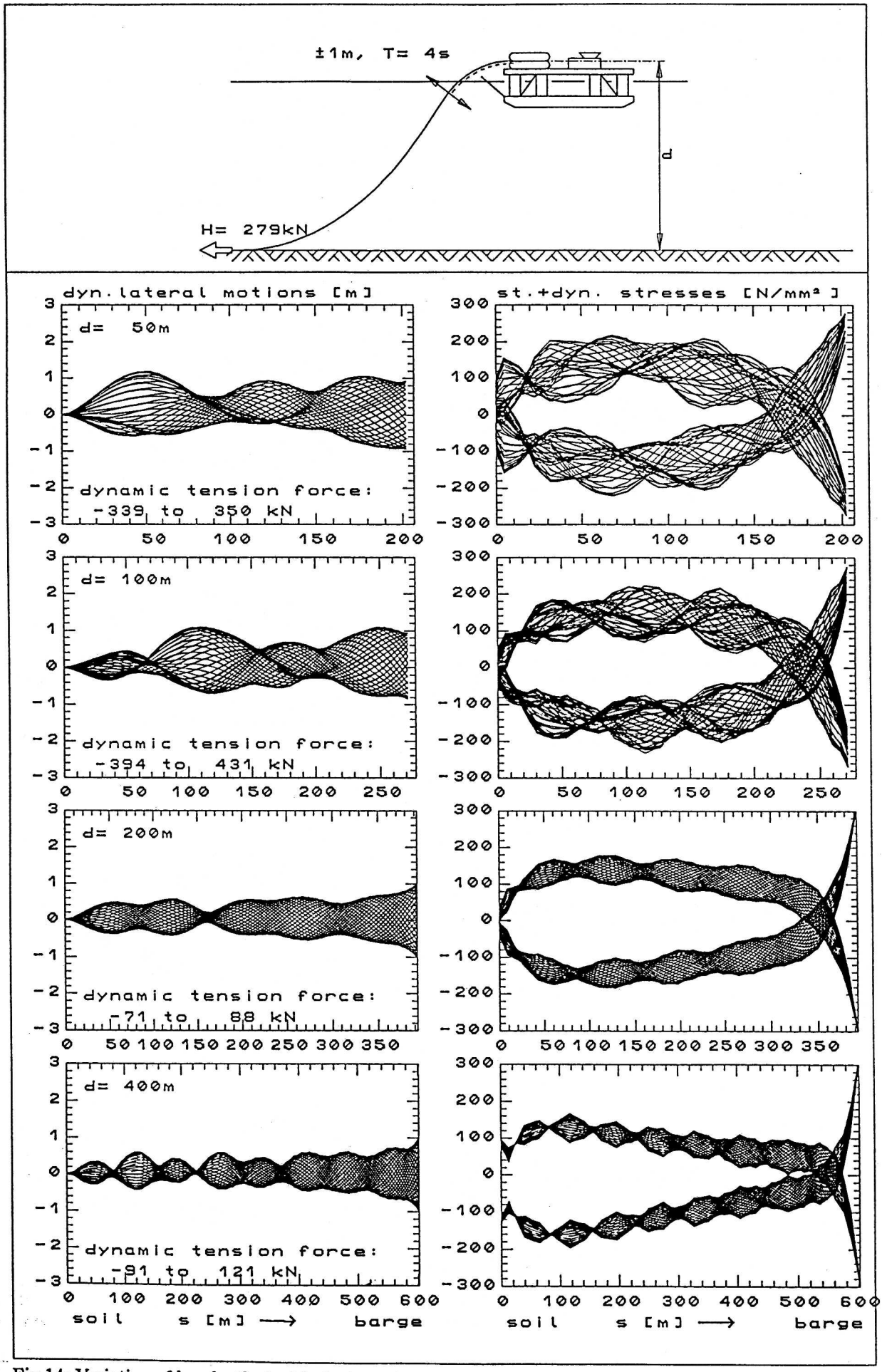

Fig.14: Variation of lay depth d – blocked tensioner

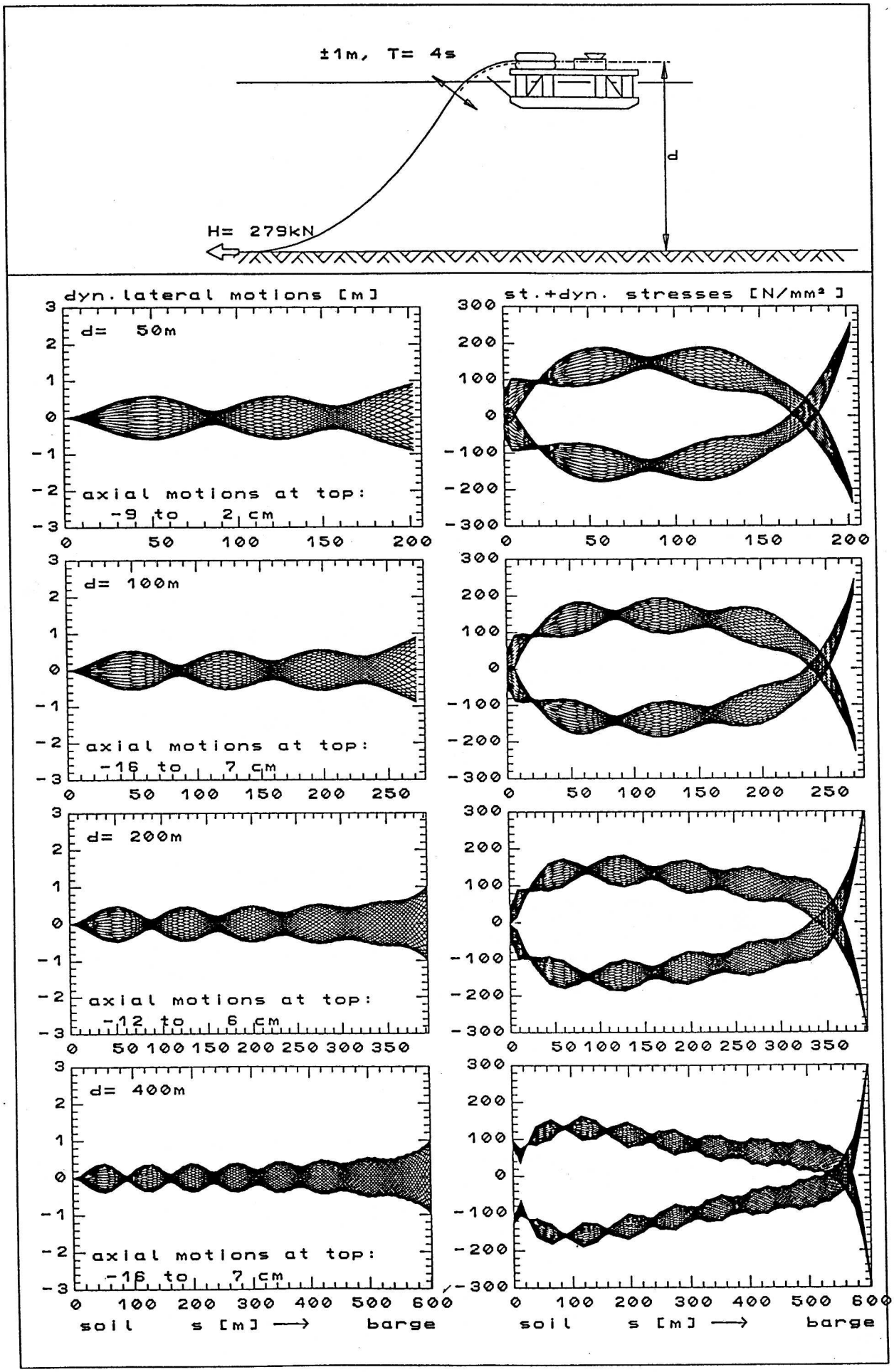

Fig.15: Variation of lay depth d – compensating tensioner